U.PORTO

FEUP FACULDADE DE ENGENHARIA
UNIVERSIDADE DO PORTO

Heat transfer enhancement in viscoelastic fluids

Luís Pedro Martins e Mendes

Supervisor:
Prof. Dr. Fernando Manuel Coutinho Tavares de Pinho

Co-Supervisor:
Prof. Dr. Alexandre Miguel Prior Afonso

A Thesis submitted for the degree of
Master of Science in Mechanical Engineering
to the Faculty of Engineering, University of Porto

Porto, March 2017

Acknowledgements

I would like to express my gratitude to Prof. Dr. Fernando M. C. Tavares de Pinho, for his excellent supervision and wealth of knowledge passed on.

To Prof. Dr. Alexandre M. P. Afonso, a profound thank you for clarifying any doubts in the process of learning the FORTRAN programming language, and for showing me the right path in the world of Computational Fluid Dynamics.

To my friends, David Magalhães and Guilherme Guedes, thank you for accompanying me in the stage of learning about viscoelasticity.

To my friends, Carlos Carneiro and Eng. Ricardo Castro, thank you for the long hours of company during the process of study and writing of this dissertation. Without you, I would not have had the same motivation.

To my friend, Eng. Rodrigo Pinto Carvalho, thank you for the ever helpful clarification of doubts about LateX programming language.

To my friend, Daniel Vieira da Silva, thank you so much for reading my dissertation, and help me improve its structure.

To my friend Mónica Faria. If it were not for you, this would not have been possible. I owe you an eternal debt of gratitude.

To my colleague, Bruno Almeida, for printing my thesis, allowing me one last read before submitting the final version of the dissertation.

To all my friends and colleagues that accompanied me during my academic years. Thank you. Your names were not mentioned, but they were not forgotten.

Your support and affection were crucial in this last phase of conclusion of my thesis. Without you, I would not have endured the presssure. To Ana Rodrigues, a special thank you. My heart belongs to you.

Last but not least, I would like to express my eternal love and gratitude to my parents and grandparents. I owe you everything. For never giving up on me, and for providing me with all the opportunities to finish my master degree.

"You, me, or nobody is gonna hit as hard as life. But it ain't how hard you hit; it's about how hard you can get hit, and keep moving forward. How much you can take, and keep moving forward. That's how winning is done."

Sylvester Stallone, in his portrayal of *Rocky Balboa*

Abstract

This work presents a numerical study on the convective heat transfer in laminar duct flow of viscoelastic fluids, to quantify the heat transfer coefficient. The study was made for the Phan-Thien and Tanner (PTT) rheological constitutive law to represent the stresses. The geometry studied was a rectangular duct with an aspect ratio of 2, assuming adiabatic vertical side walls, and heat flux imposed on the top an bottom walls. The obtained results for the heat transfer coefficient are presented in the normalized form of the *Nusselt* number (Nu).

The effect on the heat transfer coefficient was analyzed for the variation of the intensity of secondary flow, elongationality, elasticity and inclusion of a Newtonian solvent. The intensity of secondary flow was altered by varying the ξ parameter of the PTT model, in the range of ξ =[0.01, 0.05]. The effect of elongationality on the flow was studied by varying the ε parameter of the PTT model, for values of [0.1, 0.25]. Effect of elasticity was studied for *Deborah* numbers of [10, 200]. For the ratio between the solvent viscosity and the total viscosity of the viscoelastic fluid, the tested values of β_s were [0, 0.75].

The verification of the numerical method was made, by comparing the numerical results with the results obtained by analytical solutions present in the literature. The verification was carried out as a means of estimating the numerical uncertainty of the meshes used in the numerical results of this work.

The results obtained reveal that viscoelastic fluids present an enhancement of the heat transfer coefficient, when compared to Newtonian fluids. The presence of secondary flow motion has great impact on thermal entry length of the fluid. Not only does it show an asymptotic tendency to a constant value, the heat transfer coefficient exhibits a linear zone of increase, before reaching fully developed conditions.

Elongationality of the model has a very small impact on the heat transfer coefficient. Increase in elongationality causes a small increment on the heat transfer, in the presence of secondary flow. In the absence of secondary motion, elongationality has no effect on the heat transfer coefficient.

The increase of *Deborah* causes an enhancement of the heat transfer coefficient, but has no apparent effect on his thermal entrance length. In the absence of secondary flow, and without contribution of a Newtonian solvent, *Nusselt* registers an increase of 20.18%, for $De = 200$, and 8.96%, for $De = 10$. The enhancement effects caused by the presence of secondary flow on the heat transfer coefficient are smaller

with increasing values of the *Deborah* number.
Adding a Newtonian solvent contribution to the fluid has a negative impact on the heat transfer coefficient. For the tested values of β_s, with $\xi = 0$, the obtained results for the *Nusselt* number are almost the same as the Newtonian case. For smaller values of *Deborah* ($De = 10$ and $De = 20$), an enhancement of the *Nusselt* number was observed, compared to the Newtonian case, even for higher values of β_s. For higher values of *Deborah* of 100 and 200, the obtained results for Nu are the same, for all values of $\beta_s = 0.75$. It was not possible to attain convergence for $\xi \neq 0$, when $De = 100$ and 200.

In the presence of secondary flow, the *Nusselt* number registerered an increase, even when the polymer solution was dilute ($\beta_s = 0.75$). The highest increase of the *Nusselt* number was 13.4% in comparison with the Newtonian case, for $\xi = 0.05$, $\beta_s = 0.25$ and $De = 10$. For $De = 20$, the highest obtained increase in Nu was of 6.49%, for $\xi = 0.05$ and $\beta_s = 0.25$.

Resumo

Este trabalho apresentou um estudo numérico na transferência de calor convectiva em escoamentos laminares em condutas rectangulares de fluidos viscoeláticos, de forma a quantificar o coeficiente de transferência de calor. O estudo foi feito para a equação constitutiva reológica de Phan-Thien e Tanner (PTT) para prever o comportamento das tensões. A geometria estudada foi uma conduta rectangular com uma razão de forma de 2, assumindo paredes laterais verticais adiabáticas, e fluxo de calor imposto na parede de topo e parede inferior. Os resultados obtidos para o coeficiente de transferência de calor são apresentados sob a forma normalizada, o número de *Nusselt* (Nu).

O efeito no coeficiente de transferência de calor foi analisado através da variação da intensidade do escoamento secundário, elongacionalidade, elasticidade e inclusão de um solvente Newtoniano. A intensidade do escoamento secundário foi alterada fazendo variar o parâmetro ξ do modelo PTT, para a gama de valores de ξ de [0.01, 0.05]. O efeito da elongacionalidade no escoamento foi estudada fazendo variar o parâmetro ε do modelo PTT, para os valores de [0.1, 0.25]. O efeito da elasticidade foi estudado para números de *Deborah* de [10, 200]. Para o rácio entre a viscosidade do solvente e a viscosidade total do fluido viscoelático, os valores testados de β_s foram [0, 0.75].

A verificação do método numérico foi feita comparando os resultados numéricos com os resultados obtidos das soluções analíticas existentes na literatura. A verificação foi feita como forma de estimar a incerteza numérica das malhas utilizadas nos resultados obtidos neste trabalho.

Os resultados obtidos revelam que os fluidos viscoelásticos apresentam um aumento do coeficiente transferência de calor, quando comparados com fluidos Newtonianos. A presença de escoamento secundário tem um grande impacto no comprimento de entrada térmico do escoamento. Não só o *Nusselt* do escoamento apresenta uma tendência assintótica para um valor constante, como também exibe uma zona linear de aumento, antes de atingir condições completamente desenvolvidas.

A elongacionalidade do modelo tem um impacto muito pequeno no coeficiente de transferência de calor. O aumento da elongacionalidade causa um pequeno aumento na transferência de calor, na presença de escoamento secundário. Na ausência de escoamento secundário, a elongacionalidade não tem qualquer efeito no número de *Nusselt*.

O aumento do *Deborah* provoca um aumento do coeficiente de transferência de calor, mas não tem nenhum efeito aparente no comprimento de entrada térmico do escoamento. Na ausência de escoamento secundário, e sem a contribuição de um solvente Newtoniano, Nu apresenta um aumento de 20%, para $De = 200$, e 9%, para $De = 10$. Os efeitos do aumento da transferência de calor causados pela presença de escoamento secundário são mais baixos para valores mais elevados de De.

Adicionar um solvente Newtoniano ao fluido viscoelático tem um impacto negativo na transferência de calor do escoamento. Para os valores testados de β_s, com $\xi = 0$, os resultados obtidos para o número de *Nusselt* são quase iguais ao caso Newtoniano. Para valores mais baixos de *Deborah* ($De = 10$ e $De = 20$) foi observado um aumento do *Nusselt*, comparando com o caso Newtoniano, mesmo para valores mais elevados de $\beta_s = 0.75$. Para valores mais elevados de *Deborah* de 100 e 200, os resultados obtidos para o Nu são os mesmos, para todos os valores de β_s, e iguais ao caso Newtoniano. Não foi possível obter convergência para $\xi \neq 0$, para valores de $De = 100$ e $De = 200$.

Na presença de escoamento secundário, o número de *Nusselt* registou um aumento, mesmo quando a solução polimérica é diluída ($\beta_s = 0.75$). O maior aumento do número de *Nusselt* foi de 13.4% em comparação com o caso Newtoniano, para $\xi = 0.05$, $\beta_s = 0.25$ e $De = 10$. Para $De = 20$, o maior aumento conseguido para o Nu foi de 6.5%, para $\xi = 0.05$ e $\beta_s = 0.25$.

Contents

List of Figures

List of Tables

List of Symbols and Acronyms

Notation

A_c	Cross sectional area	[m^2]
AR	Aspect Ratio	[-]
b	width of the channel geometry; width of a duct geometry	[m]
c	Specific heat of the fluid	[J/KgK]
De	Deborah number	[-]
D_h	Hydraulic diameter	[m]
f	Specific function of the PTT model	[-]
f_D	Darcy friction factor	[-]
f_f	Fanning friction factor	[-]
f_x	Expansion/compression factor in the x direction	[-]
f_y	Expansion/compression factor in the y direction	[-]
f_z	Expansion/compression factor in the z direction	[-]
g_i	i component of the gravitational acceleration vector	[m/s^2]
h	half-height of the channel geometry; height of the duct geometry	[m]
h_c	Convection heat transfer coefficient	[W/m^2K]
k	Thermal conductivity of the fluid	[W/mK]
L	Characteristic length of the flow;	
	Length of the channel geometry; Length of the duct geometry	[m]
n	Power-Law index	[-]
N_1	First normal stress difference	[Pa]
N_2	Second normal stress difference	[Pa]
Nu	Nusselt non-dimensional number	[-]
p	Pressure	[Pa]
Pr	Prandtl non-dimensional number	[-]
q''	Wall heat flux	[W/m^2]
Re	Reynolds non-dimensional number	[-]
S_i	Source term in the conservation of thermal energy	[W/m^3]
S_{ij}	ij component of the deformation rate tensor	[s^{-1}]
t	Time	[s]
T	Temperature	[K]
$\bar{T}$	Average temperature of the fluid	[K]
T_w	Wall temperature	[K]
u	velocity	[m/s]
u_i	i component of the velocity vector	[m/s]
$\bar{u}$	Fluid flow average velocity	[m/s]

Greek letters

α	Parameter of the conservation of thermal energy equation;	
	Compactness parameter of the PTT channel solution	[-]
	Thermal diffusivity	[m^2/s]
β	Compactness parameter of the PTT channel solution	[-]
β_s	Ratio between the solvent viscosity and the total viscosity	[-]
δ	Compactness parameter of the PTT channel solution	[-]
$\dot{\gamma}$	Shear rate of the fluid	[s^{-1}]
ε	Elongational parameter of the PTT model	[-]
η	Coefficient of viscosity; Polymer viscosity	[Pa.s]
η_0	Zero shear rate coefficient of viscosity; total viscosity	[Pa.s]
η_p	Polymer viscosity	[Pa.s]
η_s	Coefficient of solvent viscosity	[Pa.s]
θ	Non-dimensional temperature	[-]
λ	Relaxation time of the fluid	[s]
ν	Kinematic viscosity	[m^2/s]
ξ	Slip parameter of the PTT model	[-]
ρ	Density of the fluid	[Kg/m^3]
τ_{ij}	ij component ot the stress tensor	[Pa]
$\phi(T)$	Dependency of temperature function	[-]
χ	Compactness parameter of the PTT channel solution	[-]
Ψ_1	First normal stress coefficient	[Pas^2]
Ψ_2	Second normal stress coefficient	[Pas^2]

Acronyms

CEF	Criminale, Ericksen and Filbey
CUBISTA	Convergent and Universally Bounded Interpolation Scheme for Treatment of Advection
PTT	Phan-Thien and Tanner
UCM	Upper-Convected Maxwell
UDS	Upwind Differencing Scheme

Chapter 1

Introduction

1.1 Motivation and context

This work studies the flow and heat transfer behavior of viscoelastic fluids in ducts of non-circular cross section. These viscoelastic fluids are ubiquitous in modern society and nature. Although Newtonian fluids represent in mass and volume about 99 % of the fluids present in our biosphere, there are many practical examples of fluids that exhibit viscoelastic behavior, such as blood, saliva, lubricants, cement, tooth paste, petroleum, detergents, to name a few [1].

There are many engineering applications that make use of viscoelastic fluids in their products. Common examples are the farmaceutical, cosmetic, paint, and polymer processing industries, where processing of fluids is non-isothermal, and occurs at very high temperatures. Due to this fact, proper knowledge of the temperature distribution of the fluid is needed, which provides measure for the heat transfer coefficient.

Many works have been published that observed that viscoelastic fluids present an enhancement of heat transfer when compared to fluids of Newtonian characteristics. Experimental and numerical research show that such fluids exhibit normal stresses that are not found in fluids such as water. Shear-thinning viscosity, and the existence of normal stresses, responsible for phenomena as the appearance of secondary motion and strain-hardening have been theorized to be the main cause for the increase in the heat transfer coefficient of a fluid.

To investigate the heat transfer behavior of viscoelastic fluids, an adequate rheological constitutive model has to be adopted, in order to predict the existence of normal stresses. To this aim, the Phan-Thien and Tanner (PTT) rheological constitutive law [2, 3] was chosen due to its ability to predict non-zero normal stresses arising in fluid flow. A PTT fluid also has a shear-thinning behavior, which is the common situation found in polymer melts, and aqueous polymer solutions.

1.2 Objectives

The main objective of this dissertation is to study the heat transfer behavior of viscoelastic fluids whose stresses are governed by the PTT constitutive law. A parametric study is carried out to investigate the effects of the parameters of the PTT model on the heat transfer coefficient in laminar flow in a rectangular duct with an aspect ratio of 2. The parametric study is carried out by adopting a finite volume methodology to solve the flow and heat transfer governing equations.

Initially, the effects of elongationality and secondary flow response of the PTT model are studied, with a very small contribution of a Newtonian solvent. The inclusion of Newtonian solvent is due to the fact that the test cases in study present the same properties as the ones described in the numerical work by Peres et al. [4].

Then the investigation proceeds with the analysis of the effect of the elasticity of the fluid, i.e., the effect of the *Deborah* number, and how its variation affects the heat transfer behavior of the fluid, but now assuming that there is no solvent, which is the situation for a polymer melt and in the absence of secondary flow.

Finally the parametric investigation incorporates the contribution of a Newtonian solvent without and with the presence of secondary flow, and as the *Deborah* number is progressively increased.

1.3 Thesis outline

This dissertation is divided into five chapters. The first is an introduction to the work presented. The second chapter presents a literature review on the topic of the work, namely on the numerical and experimental studies made on flow and heat transfer of viscoelastic fluids in rectangular ducts.

The third chapter presents a brief description of the numerical method used, and the meshes employed to perform the numerical simulations. A comparison with analytical cases from the literature is made to ascertain the numerical uncertainties in the calculations.

Chapter four presents results from the parametric study carried out to check the influence of the parameters of the PTT model, as well as of the contribution from the Newtonian solvent, and how they affect the heat transfer coefficient of the fluid.

The thesis ends in chapter five with the conclusions, along with suggestions for the future work in the field.

Appendix A presents the definition of the non-dimensional numbers used in this work.

Chapter 2

Literature review

In order to accurately quantify the dynamic and thermal quantities of fluid flow, proper knowledge of the laws that govern the flow and heat transfer of a fluid is needed. To this purpose, this chapter starts with a presentation of the laws of motion and heat transfer. For laminar flow of any generic fluid, it is necessary to ensure the conservation of mass, to properly state the change in momentum of the fluid, and the conservation of thermal energy must be respected. The governing laws are presented in sections 2.1, 2.2 and 2.3.

To understand the behavior of viscoelastic fluids, namely the relation between the flow kinematics and the stresses that develop in the flow, there is the need to assume a rheological constitutive law for the fluid. In this case, the Phan-Thien and Tanner constitutive model was adopted, because of its ability to predict normal stress behavior and shear-thinning, while being a relatively simple model. In this thesis, work will be done by testing the influence of secondary motion in the flow, due to the existence of normal stresses. There is a considerable amount of experimental and numerical work in the literature suggesting that secondary flow motion is responsible for the increase of laminar heat transfer behavior of fluid flow in non-circular ducts.

The main objective of this dissertation is to study the heat transfer behavior in laminar flow of viscoelastic fluids, namely the heat transfer coefficient, h_c, wich can be obtained through Newton's Law of convection (section 2.4). The heat transfer coefficient can be represented in non-dimensional form by the *Nusselt* number, *Nu*. In fully developed laminar flow of a fluid, of either viscous or polymeric nature, the *Nusselt* number tends to a constant value. For viscoelastic fluids, this non-dimensional quantity was reported to be higher than predicted for the corresponding Newtonian flow.

For this purpose, a review of experimental and numerical studies on secondary flow motions is made followed by a review of experimental and numerical works on heat transfer enhancement of viscoelastic fluids.

2.1 Conservation of mass

If the system is a fixed quantity of mass, then it means that its mass is conserved and does not change. This is called the conservation of mass. In this work, incompressibility is taken into account, and also the flow is considered to be independent of time. So if the density is constant, the conservation of mass assumes the form of equation (2.1) [1].

$$\frac{\partial u_i}{\partial x_i} = 0 \tag{2.1}$$

Equations are presented in this report in index notation, thus accounting the rule of index sum, i.e., a repeated index in a term means that it represents a sum of multiple terms.

2.2 Momentum Equation - Newton's second Law of motion for a moving fluid

If the surroundings apply a force to the fluid, Newton's second Law states that the total rate of change of momentum of the system is equal to the sum of the forces applied to it. And according to White , by applying a balance of forces to a differential element of fluid flow, the total change of momentum in that differential element assumes the form of equation (2.2) [5, 6, 7],

$$\frac{\partial \rho u_i}{\partial t} + \frac{\partial \rho u_j u_i}{\partial x_j} = -\frac{\partial p}{\partial x_i} + \rho g_i + \frac{\partial \tau_{ij}}{\partial x_j} \tag{2.2}$$

where ρ is the density of the fluid, u_i is the velocity, g_i is the gravity acceleration, and τ_{ij} is the stress tensor of the fluid. This is also called the Cauchy equation, which is valid for any fluid.

Now the only thing remaining to find is a suitable relation between the velocity field and the stress tensor. This can be done by assuming a constitutive law that describes the behavior of the stresses arising during the motion of the fluid, i.e., a rheological constitutive equation. In this thesis, it was adopted the PTT [2, 3] rheological constitutive equation.

2.2.1 PTT rheological constitutive equation

The differential model for the stresses of the fluid is given by the Phan-Thien and Tanner constitutive law [2, 3], equation 2.3,

$$\begin{gathered} \phi(T) f(\tau_{kk}) \tau_{ij} \\ +\lambda \left[\frac{\partial \tau_{ij}}{\partial t} + u_k \frac{\partial \tau_{ij}}{\partial x_k} - \tau_{jk} \frac{\partial u_i}{\partial x_k} - \tau_{ik} \frac{\partial u_j}{\partial x_k} + 2\xi \left(\tau_{jk} S_{ik} + \tau_{ik} S_{jk} \right) \right] \\ +\frac{\lambda}{\eta_p} \tau_{ik} \tau_{kj} = 2\eta_p S_{ij} \end{gathered} \tag{2.3}$$

where λ is the fluid relaxation time, η_p is the coefficient of viscosity of the polymer, and ξ is the parameter fo the PTT model responsible for a non-zero second normal

stress coefficient, i.e., the ability to predict secondary flow. The term S_{ij} is the deformation tensor, and $\phi(T)$ is a function that accounts for temperature dependent properties, and is equal to 1 if the properties are independent of temperature, which will be the case in this thesis. The dependency of properties with temperature was not studied.

$f(\tau_{kk})$ is a function that may present an exponential or linear behavior, equations (2.4) and (2.5),

$$f(\tau_{kk}) = \mathrm{e}^{\left(\frac{\varepsilon\lambda}{\eta_p}\tau_{kk}\right)} \tag{2.4}$$

$$f(\tau_{kk}) = 1 + \frac{\varepsilon\lambda}{\eta_p}\tau_{kk} \tag{2.5}$$

where ε is another PTT parameter that affects the elongational behavior of the fluid. Equation (2.4) can be accurately linearised into equation (2.5). Following the work of Peres et al. [4] the numerical simulations carried in this paper will make use of the linearized stress coefficient function of the PTT model.

2.3 Conservation of thermal energy

All heat transfer processes must obey the laws of Thermodynamics. The first law is the conservation of energy, which states that the sum of work and heat added to the system will result in an increase of the total energy of the system. In differential form, this law is in the form of equation (2.6),

$$\frac{\partial \rho C T}{\partial t} + \frac{\partial \rho C u_i T}{\partial x_i} = \frac{\partial}{\partial x_i}\left(k\frac{\partial T}{\partial x_i}\right) + \tau_{ij}S_{ij} + \mathrm{S}_i \tag{2.6}$$

where T is the temperature field, C is the specific heat and k is the thermal conductivity. S_i represents the source therm, which represents any kind of energy generation in the fluid, for example, an electrical current running through the system or any kind of internal generation of heat, while the interaction between the stress and the deformation rate tensors $\tau_{ij}S_{ij}$ represent viscous dissipation for purely viscous fluids, but in the case of viscoelastic behavior, may also include storage or dissipation of elastic energy [1].

2.4 Newton's Law of convection

To obtain the solution to the heat transfer in fluid flow, one needs to obtain the heat flux distribution applied on the boundaries of the duct, as well as the wall and fluid bulk temperatures. According to Newton, these three variables relate to each other through the heat transfer coefficient in Newton's law of convection, equation (2.7).

$$q'' = h_c(T_w - \bar{T}) \tag{2.7}$$

In this equation, T_w is the wall temperature, $\bar{T}$ is the fluid bulk mean temperature and h_c is the heat transfer coefficient. Equation (2.8) defines $\bar{T}$ (also known as the mixing cup or flow average temperature) [8]. As it can be seen, the average

temperature is integrated over the frontal area of the duct, which means it can be computed by combining the velocity and temperature fields over the cross-sectional area of the duct,

$$\bar{T} = \frac{1}{A_c \bar{u}} \int_{A_c} uT \mathrm{d}A_c \tag{2.8}$$

where A_c is the cross-sectional area of the duct (if the axial direction of the flow is x, then $A_c{=}h \cdot b$, for a rectangular duct, and $\mathrm{d}A_c{=}\mathrm{d}y \cdot \mathrm{d}z$), u is the velocity field $u{=}u(x, y, z)$, which for fully developed flow reduces to $u{=}u(y, z)$, and T is the temperature field, $T{=}T(x, y, z)$.

2.5 Brief characterization of viscoelastic liquids

To describe the flow behavior of polymeric liquids, one should represent the physical material functions of a fluid. For steady shear flow these are the shear-rate dependent viscosity, defined in equation (2.9), and the first and second normal stress coefficients, equations (2.10) and (2.11).

$$\eta(\dot{\gamma}) = \frac{\tau_{xy}}{\dot{\gamma}} \tag{2.9}$$

$$N_1 = \tau_{xx} - \tau_{yy} = -\Psi_1(\dot{\gamma}) \cdot \dot{\gamma}^2 \tag{2.10}$$

$$N_2 = \tau_{yy} - \tau_{zz} = -\Psi_2(\dot{\gamma}) \cdot \dot{\gamma}^2 \tag{2.11}$$

Several empirical models to describe non-Newtonian behavior for the stresses in a fluid have been proposed. It is of relevance to point out that there are models for purely viscous fluids, like the Power-Law [9] and Carreau-Yasuda [10, 11] models, amongst others. These useful models are derivations of the generalized Newtonian fluid definition, which deviates from the classic Newtonian fluid model by describing shear dependent viscosity, i.e., viscosity is no longer a constant, and it can increase or decrease with shear rate, also called shear-thickening or shear-thinning behavior, respectively.

The Phan-Thien and Tanner [2, 3] rheological constitutive equation, which is the object of study in this report, is a simple stress model with two parameters (ε and ξ), able to predict all three material functions presented in this section. As stated in the papers by Phan-Thien and Tanner [2] and Phan-Thien [3], these correlations provided excellent predictions for the viscosity $\eta(\dot{\gamma})$ and the first normal stress difference $N_1(\dot{\gamma})$ of low density polyethylene melts, as shown in figure 2.1.

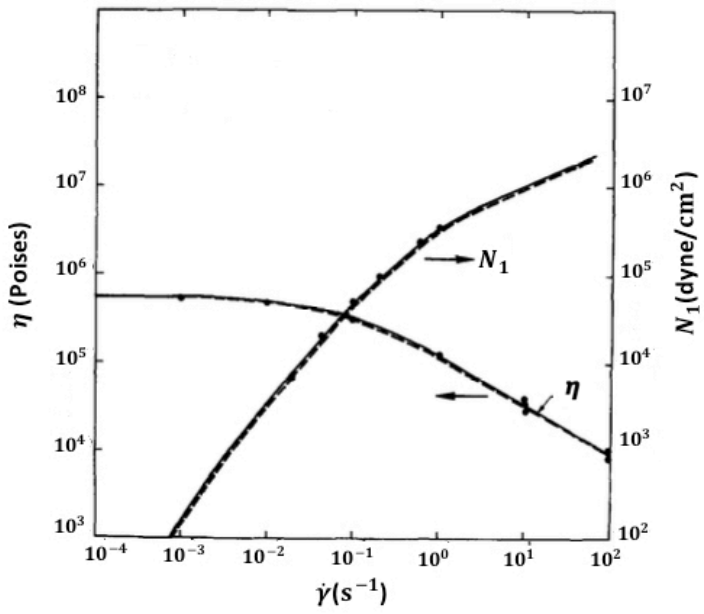

Figure 2.1: Linear PTT model fitting of the viscosity and first normal stress difference for LDPE at 150 °C. Adjustment made by Phan-Thien [2] for data extracted from IUPAC [12]. Dots are from experimental data and the lines are for the fitting curves. Adapted from the work by Phan-Thien [2].

The range in which this theory was presented in the original paper was for values of ε of 0.001 and 0.01, with a fixed value for ξ of 0.2. The ε parameter imposes a limit to the elongational rate of the fluid, which is inversely proporcional to ε. This means that, by increasing ε, the smaller the maximum elongational rate will be. The second parameter ξ causes non-zero second normal stress coefficient. It was shown by Phan-Thien et al [2] that the ratio between the second and normal stress difference is given by -$\xi/2$, so the ξ parameter of the model can also affect the other material functions of the flow.

2.5.1 Studies on stress induced secondary motion in viscoealastic fluids

The existence of secondary flow in viscoelastic fluids has been reported by many authors. Ericksen [13] and Green et al [14] theorized that, for a Reiner-Rivlin [15] type of fluid, the existence of secondary motion could in fact exist even in the case of tube flow, which was considered mathematically impossible at the time. Wheeler and Wissler [16, 17] studied the problem for the friction factor of Non-Newtonian fluids by testing laminar fluid experiments in non-circular ducts and comparing with purely viscous models. They found no evidence of elastic effects since the obtained values matched the theoretical behavior. Later, they used optical equipment to obtain the velocity field of the fluid, and they concluded that there was a slight deviation to the analytical curves of the flow, which was attributed to the existence of a weak secondary flow [18].

Several works predicted the existence of secondary motion, by solving nu-

merically the constitutive equations that predict a non-zero second normal stress difference. By comparing samples for six different viscoelastic liquids, Townsend et al. [19] were able to visualize the formation of secondary flow in those fluids. The experimental data was compared to numerical results of the Criminale-Ericksen and Filbey (CEF) [7] constitutive law , and both techniques are in agreement with each other. The main conclusion reached in Townsend et al [19] work was a clear evidence that intensity of the secondary flow is dependent on the shear rate of the fluid.

Gervang and Larsen [20] also studied the nature and magnitude of secondary flow, in a solution of 2 % viscarin in water, for different aspect ratio ducts, recurring to Laser-Doppler Anemometry. Because the intensity of the secondary flow was found to be weaker than the the primary flow, it was very hard to capture such effect. They also proceded to solve numerically the CEF [7] constitutive model to confirm and compare with their experimental results. They analysed ducts with aspect ratios of 1 up to 16, showing that there were two counter-rotating vortices in each symmetric quadrant of the duct, except for the larger aspect ratio of 16, where a third, much weaker vortex appear, as shown in figure 2.2.

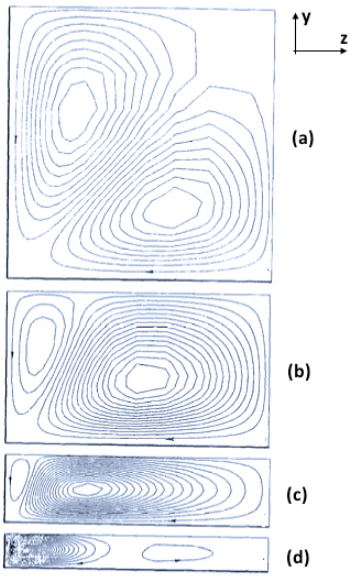

Figure 2.2: Streamlines of secondary flow in one symmetric quarter of cross section. Duct aspect ratio: (a) 1 (b) 1.8 (c) 4 (d) 16. Adapted from the work of Gervang and Larsen [20].

Gao and Hartnett [21] studied the Reiner-Rivlin [15] model, solving numerically the fluid flow for ducts with an aspect ratio of 1, 0.5 and 0.2. The streamlines of the secondary flow are presented in figure 2.3. The authors main conclusion was that the secondary flow does not influence the primary flow or the pressure drop in the fluid, and increases with the increase of the *Reynolds* number. It is also shown that is stronger in a square duct and diminishes with decreasing aspect ratio, becoming vanishingly weak for AR=5.

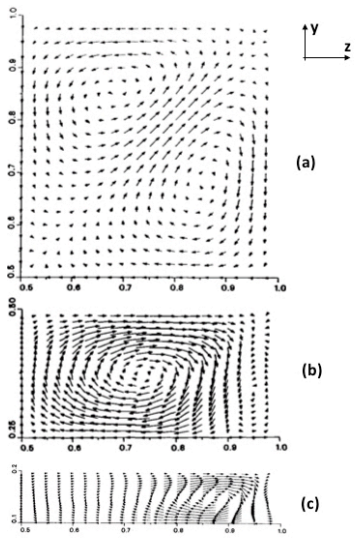

Figure 2.3: Streamlines of secondary flow in one symmetric quarter of cross section, for a Reiner-Rivlin fluid. Duct aspect ratio: (a) 1 (b) 2 (c) 5. Adapted from the work of Gao and Hartnett [21].

Similar studies were made with the PTT [2, 3] fluid, by Xue et al. [22], using a finite-volume methodology to capture the existence of secondary flow, and the corresponding numerical results are shown in figure 2.4.

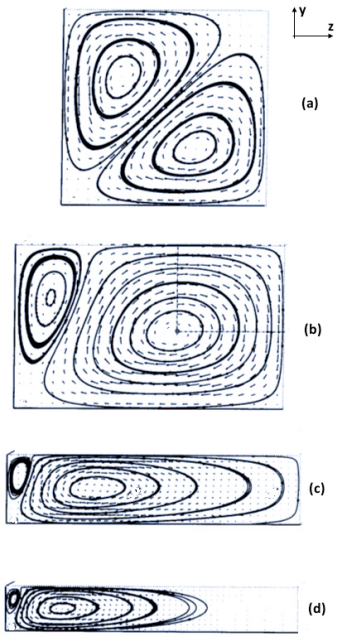

Figure 2.4: Streamlines of secondary flow in one symmetric quarter of cross section, for a PTT fluid. Duct aspect ratio: (a) 1, (b) 1.56, (c) 4, (d) 6.25. Adapted from the work by Xue et al [22].

The computations of Xue et al [22] also indicated that secondary flow implies that $\xi \neq 0$, thus allowing the existence of second normal stress difference, and the relaxation time λ of the fluid and the ε parameter of the PTT [2, 3] model have essentially no influence on the flow pattern of the secondary flow, but have strong influence on its strength, as can be seen in figure 2.5.

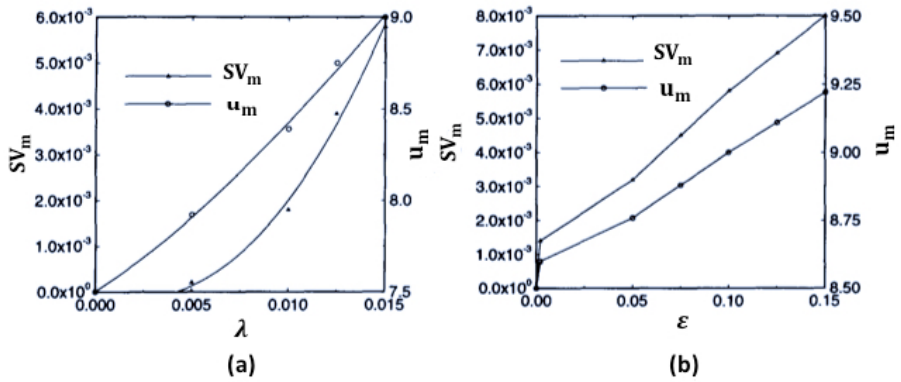

Figure 2.5: Strength of SV_m and u_m vs λ (a) and ε (b). The presented values are numerical, and the lines are fitting made. Adapted from the paper by Xue et al [22].

In figure 2.5, u_m is defined as the primary velocity, SV_m is the maximum transverse composite velocity [22], in the fully developed region, defined by equation (2.12) as a combination of the transverse velocities v and w.

$$SV_m = \sqrt{v^2 + w^2} \tag{2.12}$$

Other relevant information can be extracted from the numerical procedure carried out by Xue et al. [22]. Simulations were also made for aspect ratios of 9 and 16, and for the latter, no evidence was found of a formation of a third weak vortex, as reported by Gervang and Larsen [20]. The patterns of secondary flow were not presented in their paper, as it was reported that the ratios were too large to plot out. Also, the increase of either the relaxation time λ of the fluid and the elongational parameter ε of the PTT [2, 3] model contribute to an increase of both the intensity of the secondary flow and the primary velocity.

2.5.2 Heat transfer enhancement in viscoelastic fluids

For the Phan-Thien and Tanner constitutive law [2, 3], the energy equation is also presented in a modified way, with a contribution of a Newtonian solvent (η_s), as shown by equation (2.13),

$$\begin{aligned} &\frac{\partial \rho C T}{\partial t} + \frac{\partial \rho C u_i T}{\partial x_i} \\ &= \frac{\partial}{\partial x_i}\left(k\frac{\partial T}{\partial x_i}\right) + \eta_s\left(\frac{\partial u_i}{\partial x_j} + \frac{\partial u_j}{\partial x_i}\right)\frac{\partial u_i}{\partial x_j} + \alpha\tau_{ij}\frac{\partial u_i}{\partial x_j} + (1-\alpha)\,\frac{\tau_{kk}}{2\lambda}f(\tau_{kk}) \end{aligned} \tag{2.13}$$

where the term proportional to η_s includes the effect of viscous dissipation by the Newtonian solvent, whereas the last two terms account for mechanical energy suply by the PTT fluid. The term $\alpha\tau_{ij}\frac{\partial u_i}{\partial x_j}$ represents viscous dissipation by the polymer, and the term $(1-\alpha)\frac{\tau_{kk}}{2\lambda}f(\tau_{kk})$ quantifies the energy that is stored elastically as internal energy to be released later. As demonstrated by Peters et al. [23] on their numerical simulations on the benchmark case of flow around a confined cylinder, it was shown that the effect of the parameter α is fairly small on the temperature profile. The results are very similar for α=0 or α=1. Also, as shown by Wapperom [24] and by Wapperom et al. [25], in fully developed shear flow there is no internal energy storage and only viscous dissipation is of importance, which is mathematically equivalent to α=1.

It has been shown that viscoelastic fluids present an enhancement of the heat transfer coefficient comparatively to a fluid of Newtonian characteristics. Several works are available in the literature for the cases where the fluids are assumed as purely viscous, i.e., normal stress behavior cannot be predicted. Metzner [26] and Hartnett et al. [27] made an extensive review on the literature available for these types of constitutive stress models. The general conclusions are that the heat transfer coefficient, for fully developed flow of shear-thinning fluids is bigger than what is reported for the Newtonian case.

By adopting a purely viscous constitutive model (Power-Law [9] fluid with n=0.6), Hartnett and Kostic [28] performed experimentations on aquous polymer solutions. The geometry was a duct with an aspect ratio of 2, with both upper and lower walls being heated. Their results confirmed an increase in the *Nusselt* number, by comparison with water. In the experimentations on both types of fluids, the heat transfer coefficient presented unequal values for both walls. As observed in the case of water, it was shown that the upper wall *Nusselt* number was in good agreement with the analytical solution reported by Wibulswas [29]. Wibulswas did not consider effects of buoyancy in his solution. It is not then surprising that the upper wall values match the analytical values, because the effects of gravity on the upper wall are logically much less intense than on the bottom. By comparing with the viscoelastic experiments, the main conclusion from Hartnett and Kostic [28] experimental data was that natural convection in these cases merely redistributed the heat transfer coefficient, and the increase of the *Nusselt* number was probably due to secondary flow arising in the measured experiments, as the tested fluid was a very dilute solution, with weak elasticity.

Rao [30] also observed an increase in the *Nusselt* number, for a duct with an aspect ratio of 5. The experimental set-up was the same as the experimental work carried out by Hartnett and Kostic [28], and in this case the reported heat transfer coefficient was much lower than in the case for the duct with $AR = 2$, but still higher than water.

As described here in this thesis, several numerical works have been carried out to test the magnitude of secondary flow with varying aspect ratio. And as shown in those numerical works [20, 21, 22], with increasing aspect ratio, the strength of the secondary flow in the fluid decreases. It is reasonable to assume that existence

of a second normal stress coefficient on a viscoelastic fluid has a positive influence on the heat transfer coefficient, and its effects are as intense as the intensity of the secondary flow occurring during fluid motion.

Gao and Hartnett [31] performed numerical simulations by adopting the Reiner-Rivlin [15] constitutive model for the stresses, which is able to predict a non-zero second normal stress coefficient. In their paper, several boundary conditions were tested for wall heating, and in all cases the reported values exhibit an enhancement of the *Nusselt* number by comparison to purely viscous shear-thinning fluids.

Payvar [32] adopted the CEF [7] constitutive model to numerically predict the behavior of the experimental data obtained by Kostic [33] for a duct with the same geometry and boundary conditions as the ones described by Hartnett and Kostic [28]. The results showed a good match to the experimental values, and it was observed that the axial *Nusselt* number, after decreasing asymptotically, it shows a behavior of linear growth, which is then followed by another asymptotic decrease to a constant value, along the axial direction of the flow. According to the results obtained by Payvar, the *Nusselt* number shows a large enhancement when compared to a Newtonian fluid, and the thermal entrance length is also much higher.

Peres et al. [4] performed numerical simulations by adopting the Phan-Thien and Tanner [2, 3] constitutive law to model the behavior of the stresses of the fluid. The PTT model is also able to predict all the material functions presented in section 2.5. With the inclusion of buoyancy effects in the flow, Peres et al. [4] were able to predict the behavior of the specimens tested by Hartnett and Kostic [28] in their experimental work, assuming the same geometry (duct with an aspect ratio of 2) and thermal boundary conditions (upper and lower walls heated, side walls were considered adiabatic). Similarly to the previous works, the conclusion was that buoyancy only introduces a redistribution effect on the heat transfer coefficient on the heated walls, while the enhancement of the heat transfer coefficient is mainly due to the occurence of secondary flow arising from a non-zero second normal stress coefficient ($\xi \neq 0$).

2.6 Summary and outlook

In this chapter, a review on viscoelastic fluids thermal and dynamic flow behavior is presented. As reported in the literature, viscoelastic fluids present a clear enhancement on the heat transfer coefficient.

In order to test the influence of viscoelasticity on the heat transfer behavior in fluid flow, a parametric study will be performed. The fluid is governed by the PTT constitutive law to model the stress behavior. The flow in study is laminar, with no effects of buoyancy, under steady state conditions (no time dependency).

Several studies have been made on the heat transfer behavior of PTT fluids in channel flow. Pinho and Oliveira [34] derived the analytical solution for channel flow of the PTT fluid subjected to constant wall heat flux. Coelho et al [35] derived

the analytical solution for the case where constant wall temperature was imposed. However, there is no known analytical solution for the case of rectangular ducts. Incidentally, the numerical studies in this thesis were made for rectangular ducts. Given that a previous numerical study on heat transfer behavior was made by Peres et al. [4], the duct will have an aspect ratio of 2, which was chosen by the authors to compare with the experimental work carried by Hartnett and Kostic [28].

In the numerical work carried out by Peres et al. [4], focus was made on the effect of the ξ parameter of the PTT model to study the influence of secondary motion on the heat transfer behavior of the fluid. No variation of the elongational parameter was made to check the influence on heat transfer. Consequently, the ε parameter of the PTT model was tested in this thesis to check its influence on the heat transfer behavior of the fluid.

Test cases C, D and E presented by Peres et al [4] had the same *Deborah* number. As a consequence, elasticity was assumed constant in the numerical work by Peres et al. [4]. The influence of the *Deborah* number is going to be tested to check if the heat transfer coefficient will remain constant, or if it depends on *De*.

Test cases C, D and E had a small contribution of a Newtonian solvent (the Newtonian solvent coefficient of viscosity, η_s, was of 0.0055). To check the influence of Newtonian solvent contribution, different quantities of β_s (defined in appendix A) were tested to check the influence on the heat transfer coefficient.

Results were obtained for *Deborah* numbers of 100 and 200. Because convergence could not be obtained for the cases where $\xi \neq 0$, only the results for Newtonian solvent contribution is presented for those cases.

To finish the parametric study, the combined effects of varying elasticity (De), Newtonian solvent contribution (η_s), and secondary flow intensity (ξ) was tested to check the influence of these parameters on the heat transfer behavior of the fluid.

Chapter 4 presents the results for the heat transfer coefficient in normalized form, as the *Nusselt* number. Before proceeding to the final results, the finite volume methodology implemented to run the simulations was tested and compared with several analytical solutions, as a means of estimating the numerical error associated with the numerical method used, and the meshes employed to run the cases. The comparisons made are presented in chapter 3.

Chapter 3

Numerical method and validation of results

This chapter starts with a brief overview of the validation made by the authors of the simulation code, followed by a presentation of the discretized equations of the finite volume method used, and the meshes employed in the numerical runs. Several verifications on the numerical uncertainties are made, by comparing with the analytical solutions available for channel flow of Newtonian fluids, and PTT fluids with zero and non-zero second normal stress difference. To conclude, tests on 3D meshes are made by comparing the obtained *Nusselt* number with the theoretical values. The chapter finishes with a discussion of the results obtained in the verification of the code.

3.1 Brief Overview

The present code has been continuously altered throughout the years, and it was first implemented by Oliveira et al. [36]. The purpose of the work carried out by the authors of the paper was the extension of the finite volume method to deal with viscoelastic fluids. The code developed allows the simulation of both 2D and 3D cases, and the meshes may be non-orthogonal and semi-structured in order to adapt to any arbitrary flow-boundary geometry.

The validation of the code was carried out for two different cases. For the first case, 2D channel slip-stick entry flow for an Upper-Convected Maxwell (UCM) [7] model, which was compared with results reported by Eggleton et al [37], and both works are in good agreement with each other. The second test was made for the case of a fluid flowing around a circular cylinder in a channel, compared with several other works reported in the literature, and the results are in agreement with the ones reported in references [38, 39, 40].

The inclusion of the energy equation was made later by Nóbrega et al [41]. In the paper by Nóbrega et al [41], a thorough investigation was made for the simplified version of the PTT model (SPTT, ξ=0). The validation of the code was made by simulating the *Graetz-Nusselt* problem for a Newtonian fluid, to which semi-analytical solutions can be found in Shah and London [42], and for the SPTT

model, where the analytical solution can be found in detail in the paper published by Coelho et al. [43]. The results match almost exactly the analytical solutions found in the literature.

3.2 Numerical method

In finite volume methodology, the domain of calculation is divided into a given number of cells. In each cell, or control volume, the flow and heat transfer of the fluid occuring in that domain are calculated. For that purpose, the governing equations are discretized. This means that the derivatives are substituted by finite differences, thus turning the equations of state into a set of algebraic functions. The cell in which the governing equations are being calculated is denoted as cell P, while the others are defined in geographic notation, as shown in figure 3.1.

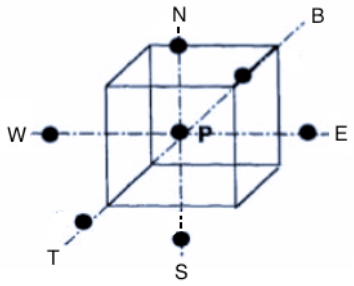

Figure 3.1: Convention of the faces for a control volume in finite volume methodology. W (west), E (east), S (south), N (north), B (bottom), T (top). Adapted from the doctoral thesis of Cavadas [44].

As referred previously, the mesh used in the calculations is block-structured and non-orthogonal and all the variables are calculated on the centre of each computational cell (collocated mesh). This poses an issue because as the pressure and velocity fields are directly dependent from one another, then the pressure should be calculated in a different mesh than the one for the velocity field, to guarantee the coupling between both. With a collocated mesh, such thing is not possible, and for that reason it is necessary to introduce a pressure correction algorithm that is described in the work by Rhie et al. [45].

3.2.1 Conservation of mass

The conservation of mass is discretized in the form of equation (3.1),

$$\sum_{f=1}^{6} F_f = 0 \tag{3.1}$$

where F_f represents the mass flux that leaves the face f and the sum is made for the six faces of each cell, taking on a positive value if the flux is leaving the cell and a negative one if it means an entrance to the control volume.

3.2.2 Momentum equation

For the conservation of momentum, the discretized form of the equation for a given cell P and with a volume V_P takes on the form of equation (3.2),

$$a_p u_{i,p} - \sum_F a_F u_{i,F} = S_{u_i} + \frac{\rho V_P}{\delta_t} u^0{}_{i,p} \tag{3.2}$$

where δ_t represents the time step and $u^0{}_{i,p}$ represents the velocity calculated in the previous time step. a_F represents the flux contributions from neighbouring cells, and is separated in both a convective and diffusive term, a_F=$a^C{}_F$+$a^D{}_F$. For the convective term, Oliveira et al. [36] stated that, according to upwind differencing scheme (UDS) that calculation is made in the following way:

$$a_F^C = -F_f^- = -min(F_f, 0) \quad \text{for a positive face, } f^+ \tag{3.3a}$$

$$a_F^C = +F_f^+ = +max(F_f, 0) \quad \text{for a negative face, } f^- \tag{3.3b}$$

and for the diffusive term, it is calculated as presented in equation (3.4).

$$a_F^D = (\eta_s + \eta_{p,f}) \frac{B_f^2}{V_f} \tag{3.4}$$

The central coefficient a_P and the source term are given by equations (3.5) and (3.6).

$$a_p = \frac{\rho V_P}{\delta t} + \sum_{f=1}^{6} a_f \tag{3.5}$$

$$S_{u_i} = S_{u_i \ \substack{\text{Newtonian} \\ \text{diffusion}}} + S_{u_i \ \text{pressure}} + S_{u_i \ \substack{\text{extra} \\ \text{tensor}}} + S_{u_i \ \substack{\text{artificial} \\ \text{diffusion}}} + S_{u_i \ \text{HRS}} \tag{3.6}$$

In equation (3.6), $S_{u_i \ \substack{\text{Newtonian} \\ \text{diffusion}}}$ represents the term due to a purely Newtonian contribution to the stress tensor, $S_{u_i \ \text{pressure}}$ is the contribution from the pressure gradient acting in the flow, $S_{u_i \ \substack{\text{extra} \\ \text{tensor}}}$ represents the non-Newtonian (elastic or inelastic) contribution to the stress tensor, $S_{u_i \ \substack{\text{artificial} \\ \text{diffusion}}}$ is the contribution from the artificial diffusive term added by Oliveira et al. [36] in the conservation of momentum to promote stability to the finite volume methodology, and $S_{u_i \ \text{HRS}}$ represents the contribution due to the use of a high resolution scheme, CUBISTA, developed by Alves et al. [46]. This last source term accounts for the difference between the convective terms calculated using the UDS and the CUBISTA schemes.

3.2.3 Conservation of thermal energy

The discretized form of the energy equation takes the form of equation (3.7).

$$a_p T_p - \sum_F a_F T_F = S_T + \frac{\rho c V_P}{\delta_t} T^0{}_p \tag{3.7}$$

As can be seen, its form is very similar to the form of the momentum equation. The only difference being that the temperature is a scalar quantity, and not a vector quantity like the velocity. ${T^0}_p$ represents the temperature calculated at the previous time step. The central coefficient a_P is as follows in equation (3.8).

$$a_p = \frac{\rho C_P V_P}{\delta t} + \sum_{f=1}^{6} a_f \tag{3.8}$$

The diffusive coefficient ${a^D}_F$ may take two forms:

$${a^D}_F = \frac{k_f}{V_f} B_{lj} B_{mj} \begin{cases} a_f^{DN} & \text{if l=m or} \\ a_f^{DC} & \text{if l} \neq \text{m} \end{cases} \tag{3.9}$$

The diffusive coefficient needs to be splitted because $a_F = a_F^C + a_F^{DN}$ and the convective coefficient is calculated according to UDS as follows next,

$$a_F^C = -C_P F_f^- = -C_P min(F_f, 0) \quad \text{for a positive face, } f^+ \tag{3.10a}$$

$$a_F^C = +C_P F_f^+ = +C_P max(F_f, 0) \quad \text{for a negative face, } f^- \tag{3.10b}$$

and for the discretized source term, it is given by equation (3.11).

$$S_T = -\sum_P a_F^{DC} \left(T_P - T_F\right) \tag{3.11}$$

3.2.4 PTT constitutive equation

The discretized form of the PTT constitutive equation is in the form of equation (3.12),

$$a_p^\tau \tau_{ij,p} - \sum_F a_F^\tau \tau_{ij,F} = S_{\tau_{ij}} + \frac{\lambda V_P}{\delta_t} {\tau^0}_{ij,p} \tag{3.12}$$

where the coefficients a_F^τ only include a convective component, due to the inexistence of a diffusive term in the constitutive equation, and the coefficient a_p^τ is calculated by equation (3.13),

$$a_p^\tau = V_P \left(1 + \frac{\lambda_P}{\delta_t} + \frac{\alpha \lambda_P}{\eta_p, P} \sum_{k=1}^{3} \tau_{kk,P}\right) + \sum_{f=1}^{6} a_F^\tau = 0. \tag{3.13}$$

3.3 Verification of results

The numerical method was tested to check the performance of the dynamics and heat transfer behavior of laminar channel flow for a Newtonian fluid, and for a viscoelastic fluid governed by the PTT constitutive law, with zero second normal stress difference coefficient. The dynamic behavior of laminar flow in channel for the case where $\xi \neq 0$ was also tested, although no thermal solution exists. The latter was tested to check the influence of the ξ parameter of the PTT model, and how it would affect the numerical results.

Analytical solutions for laminar channel flow of a Newtonian fluid can be found in several textbooks in fluid mechanics and heat transfer [5, 6, 8, 42]. The fluid dynamics and heat transfer behavior for laminar channel flow of SPTT fluids can be found in the articles by Oliveira et al. [47] and Pinho et al. [34], for the dynamics and heat transfer behavior, respectively. For the complete PTT model ($\xi \neq 0$), only a partial solution exists, and detailed description can be found in the paper by Alves et al. [48].

Because the tests for the heat transfer behavior of the PTT model were made in rectangular ducts, verification was also made for 3D geometries by comparing the numerical results with the analytical solutions for laminar Newtonian duct flow, where detailed analytical solutions for the *Nusselt* number can also be found in any textbook on heat transfer [42, 8].

3.3.1 Meshes used in the numerical simulations

This section presents the meshes used in the simulations carried out in this work. The first trials were simulations for a 2D geometry, considering a length L of 6.4 m, a height h of 9 mm (having a hydraulic diameter of 18 mm), with an infinite width b (which is equivalent to employ only one cell with symmetry imposed on both sides of the spanwise direction z). The meshes used for the case of channel flow are summarized in table 3.1.

Table 3.1: Meshes used in the simulations for channel flow

Meshes	N_x	N_y	δ_x/D_h	δ_y/D_h	f_x,f_y
CA	800	10	0.444	0.025	1,1
CB	800	20	0.444	0.0125	1,1

For these two meshes, symmetry was imposed along the the centerline of the channel, so only half of the physical domain was employed. Mesh CA was used for the Newtonian case, and to check if more accurate results could be obtained for the tests concerning viscoelastic fluids, the vertical direction y was refined with the double of cells reported, thus mesh CB was used for the comparison with the PTT models.

For the case of 3D simulations, three different meshes were used. Following the experimental work carried out by Hartnett and Kostic [28], and the numerical procedure carried out by Peres et al [4], the flow geometry is a duct with an aspect ratio of 2, with an height h of 9 mm, and a width b of 18 mm, which means the hydraulic diameter was of 12 mm. This is the equivalent of mesh DA in table 3.2.

Mesh DA was only used to test the response of the models reported in the article by Peres et al [4], and the results are given in chapter 4. The length L of the physical domain was of 6.4 m. For the remaining results, the mesh used had half the length of mesh DA, $L = 3.2$ m. This was employed in meshes DB and DC, and the accuracy of these meshes was tested for laminar flow of Newtonian fluid. The difference between the two is the aspect ratio. Mesh DB had an aspect ratio of 2, the same of mesh DA, whereas for mesh DC the aspect ratio was of 1. The height and width of the duct was of 9 mm, thus defining an hydraulic diameter of 9 mm.

In the case of 3D meshes, only a quarter of the flow physical domain was simulated, which is equivalent to set two symmetry planes, one on the vertical direction y and another on the spanwise direction z.

Table 3.2 presents a summary of the characteristics of the 3D meshes employed in this work.

Table 3.2: Meshes used in the simulations for duct flow

Meshes	N_x	N_y	N_z	δ_x/D_h	δ_y/D_h	δ_z/D_h	f_x,f_y,f_z
DA	800	10	20	0.667	0.0375	0.0375	1,1,1
DB	800	10	20	0.333	0.0375	0.0375	1,1,1
DC	800	10	10	0.444	0.05	0.05	1,1,1

3.3.2 Flow of a fluid in a channel

The objective here is to analyze the flow a fluid between two parallel plates (channel), that are distanced from each other by a distance of $2h$, and the axial direction is the x direction, as can be seen by figure 3.2. The centerline, where symmetry is imposed, is located at $y = 0$. The flow is considered time independent, and as the z direction is considered infinite, the gradients in that direction are neglected, wich means w=0. Due to the no-slip condition at each wall, it can also be concluded that v is also zero. To conclude, the buoyancy effect is neglected in the momentum balance.

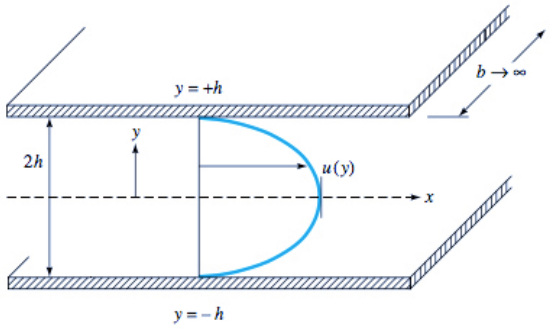

Figure 3.2: Parallel plates geometry, and illustrative example of the velocity profile of a generic fluid. Adapted from White [5].

3.3.2.1 Newtonian channel flow

The solution to velocity profile $u(y)$ is given by equation (3.14) [5, 6, 7].

$$u(y) = \frac{\partial p/\partial x}{2\eta}(h^2 - y^2) \tag{3.14}$$

The numerical simulations in this work are defined based on the average velocity of the flow, and not the pressure gradient. Because of this issue, it is necessary to establish a relation between both. According to White [5], the average velocity is defined by integrating the velocity profile and dividing it by the cross-sectional area of the flow,

$$\bar{u} = \frac{2}{bh}\int_0^h u(y) b \mathrm{d}y \tag{3.15}$$

$$\bar{u} = \frac{\partial p}{\partial x}\frac{h^2}{3\eta} \tag{3.16}$$

and substituting equation (3.16) into equation (3.14), the velocity profile is expressed as a function of the average velocity:

$$u(y) = \frac{3}{2}\bar{u}(h^2 - y^2) \tag{3.17}$$

The corresponding shear stress of the fluid is given by Newton's Law of viscosity,

$$|\tau_{xy}| = \eta\left|\frac{\partial u}{\partial y}\right| = 3\bar{u}\eta y \tag{3.18}$$

where $\eta = \eta_s$. Since the results will be presented in normalized form, we will take $u^* = u(y)/\bar{u}$ and the characteristic length L will be assumed as the half-width of the channel, h, thus making $y^* = y/h$, and the shear stress is normalized with the wall shear stress ($3\eta\bar{u}h$). The normalized velocity and shear stress profiles are as follows:

$$u^* = \frac{3}{2}\left(1 - y^{*2}\right) \tag{3.19}$$

$$|\tau_{xy}|^* = \frac{\tau_{xy}}{3\eta\bar{u}/h} = y^* \tag{3.20}$$

To test the validity of the code, simulations were carried out according to the geometry used in the work of Peres et al. [4]. The length and height where the same as the duct simulated by Peres et al. [4], except the bottom and top direction only has one single cell. The tested *Reynolds* was of 20 with a *Prandtl* of 6.4, without inclusion of natural convection effects and with an imposed heat flux of 240 W/m^2. For a Newtonian fluid, the properties are summarized in table 3.3.

Table 3.3: Properties simulated for Newtonian channel flow

Property	Value	Unit
ρ	1000	$[W/m^2]$
η	1×10^{-3}	[Pa.s]
C	3904	[J/KgK]
k	0.61	[W/mK]
$\bar{u}$	1.1×10^{-3}	[m/s]

The analytical functions were then compared with the corresponding simulated values, and the results are presented in figures 3.3 and 3.4 for the velocity and shear stress profiles.

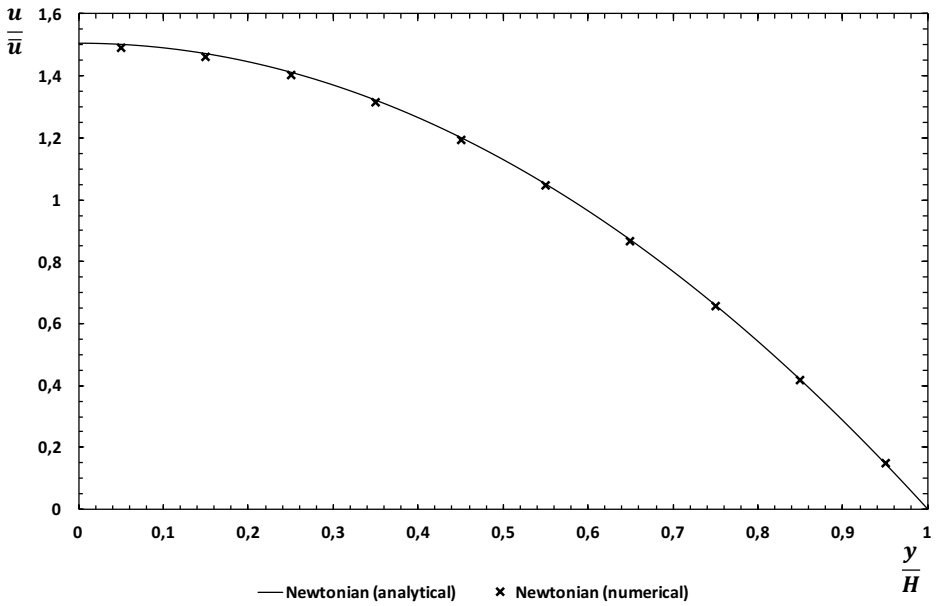

Figure 3.3: Analytical and numerical values for the velocity profile in Newtonian fluid flow.

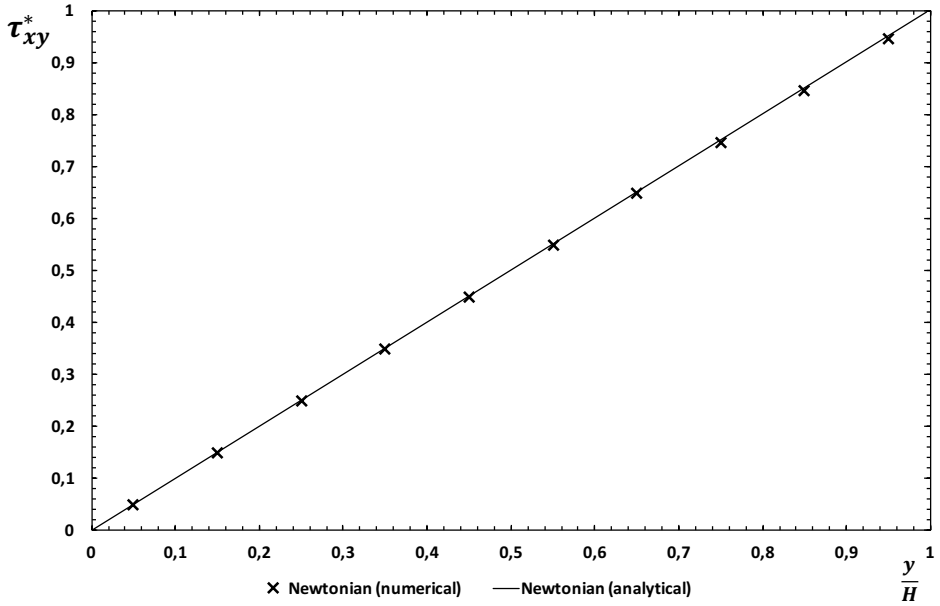

Figure 3.4: Analytical and numerical values for the shear stress profile in Newtonian fluid flow.

For the heat transfer analysis, it was assumed flow without viscous dissipation and assuming fully developed and steady state conditions. The solution for the temperature profile, according to Shah and London [42], with equal heat fluxes on the walls of the channel, is given by equation (3.21).

$$T(y) = T_w - \frac{3}{2}\frac{q''}{hk}\left(\frac{5h^2}{12} - \frac{y^2}{2} + \frac{y^4}{12h^2}\right) \tag{3.21}$$

The use of equation (2.8) together with equations (3.14) and (3.21) results in the average temperature for this flow problem,

$$\bar{T} = T_w - \frac{17}{140}\frac{q''D_h}{k} \tag{3.22}$$

where $D_h = 4h$ for the case of channel flow.

Equation (3.22) is useful because the temperature distribution is going to be normalized, producing the following result, equation (3.23).

$$\theta(y) = \frac{T(y) - T_w}{\bar{T} - T_w} = \frac{105}{34}\left(\frac{5}{12} - \frac{y^{*2}}{2} + \frac{y^{*4}}{12}\right) \tag{3.23}$$

Following Newton's law of convection (equation (2.7)), the heat transfer coefficient h_c, in normalized form of the *Nusselt* number, is 8.235. Figure 3.5 presents the comparison between the analytical and numerical temperature profiles, and figure 3.6 shows the asymptotic tendency of the axial *Nusselt* number to its corresponding analytical value for fully developed flow.

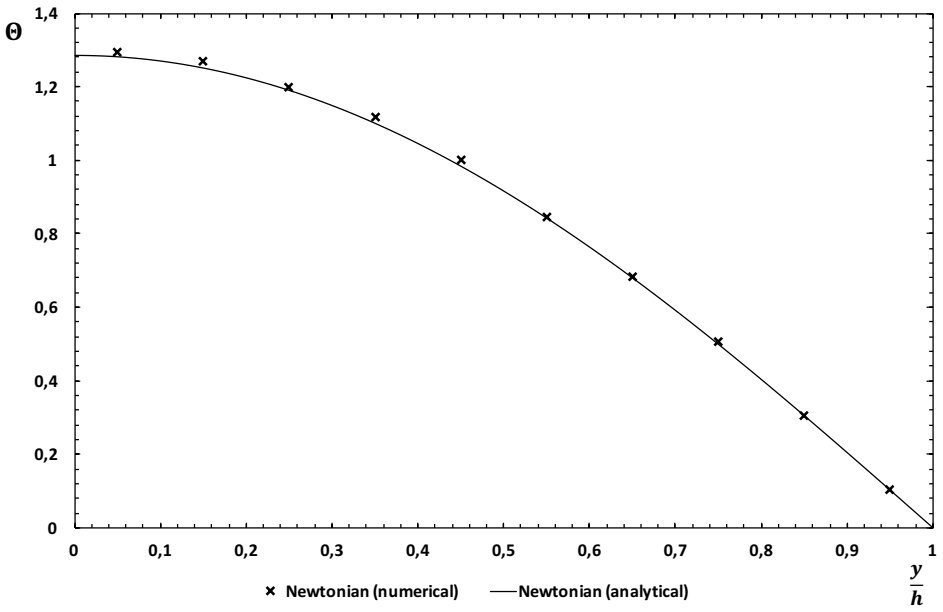

Figure 3.5: Analytical and numerical values for the temperature profile in Newtonian fluid flow.

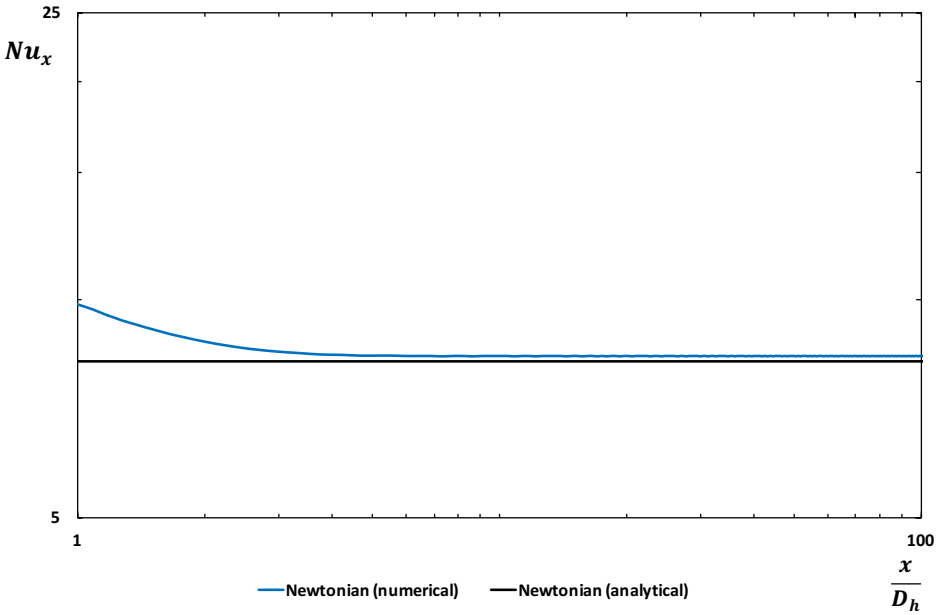

Figure 3.6: Asymptotic tendency for the Nusselt number to the corresponding analytical value for fully developed conditions, along the channel.

3.3.2.2 Simplified version of the Phan-Thien and Tanner fluid

We take upon the analytical solution derived by Pinho and Oliveira [47] for the Phan-Thien and Tanner fluid with zero second normal stress difference ($\xi = 0$), also called SPTT. In this work, and as referenced before, we are merely interested in analysing the linearized form of the specific function f (equation (2.5)).

As we are analysing fully developed flow, then the velocity and stresses only depend on the lateral coordinate y. And combining the conservation of mass (equation (2.1)) with no-slip condition at the wall, then it can be concluded that v=0. The present solution does not take into account contribution of a Newtonian solvent to the stresses, so $\eta_s = 0$ (making $\eta_p = \eta$). With these simplifications, the analytical solution is derived, and the results for the velocity u, shear stress τ_{xy} and normal stress τ_{xx} profiles is given by the following set of equations:

$$u(y) = -\frac{\partial p/\partial x}{2\eta}\left(h^2 - y^2\right)\left(1 + \frac{\varepsilon\lambda^2(\partial p/\partial x)^2}{\eta^2}\left(h^2 + y^2\right)\right) \tag{3.24}$$

$$\tau_{xy} = \frac{\partial p}{\partial x}y \tag{3.25}$$

$$\tau_{xx} = \frac{2\lambda}{\eta}\left(\frac{\partial p}{\partial x}\right)^2 y^2 \tag{3.26}$$

The average velocity can be computed by equation (3.15) to yield the following expression,

$$\bar{u} = -\frac{(\partial p/\partial x)\, h^2}{3\eta}\left(1 + \frac{6\varepsilon\lambda^2(\partial p/\partial x)^2 h^2}{5\eta^2}\right) \tag{3.27}$$

and the normalized profile velocity is as follows in equation (3.28). The pressure is scaled with $\eta\bar{u}/h$ and the lateral coordinate y is scaled with the half-width of the channel, h. The *Deborah* number is defined not based on the hydraulic diameter, but on the half-width of the channel, thus producing $De = \frac{\lambda\bar{u}}{h}$.

$$u^* = \frac{3}{2}\frac{\bar{u}_N}{\bar{u}}\left(1 - y^{*2}\right)\left(1 + 9\varepsilon De^2\left(\frac{\bar{u}_N}{\bar{u}}\right)^2\left(1 + y^{*2}\right)\right) \tag{3.28}$$

In equation (3.28) $\frac{\bar{u}_N}{\bar{u}}$ is a dimensionless pressure gradient, and $\bar{u}_N$ corresponds to the cross-sectional average velocity for a Newtonian fluid, wich is given by equation (3.16). Pinho and Oliveira [47] derived a very useful expression for $\frac{\bar{u}_N}{\bar{u}}$, wich will be presented here in equation (3.29). A detailed explanation on how the dimensionless pressure gradient is obtained can be found in [47].

$$\frac{\bar{u}_N}{\bar{u}} = \frac{(432)^{1/6}\left(\delta^{2/3} - 2^{2/3}\right)}{6b^{1/2}\delta^{1/3}} \tag{3.29}$$

In equation (3.29), b and δ are compactness parameters to help simplify the expression, and are determined by expressions (3.30) through (3.33).

$$b = \frac{54}{5}\varepsilon De^2 \tag{3.30}$$

$$\delta = \alpha^{1/2} + \beta \tag{3.31}$$

$$\alpha = 3^3 b + 4 \tag{3.32}$$

$$\beta = 3^{3/2} b^{1/2} \tag{3.33}$$

The normalized shear stress τ_{xy} and normal stress τ_{xx} are obtained by scaling equations (3.25) and (3.26) with the wall shear stress for a Newtonian fluid, $3\eta\bar{u}/h$.

$${\tau_{xy}}^* \equiv \frac{\tau_{xy}}{3\eta\bar{u}/h} = -\Big(\frac{\bar{u}_N}{\bar{u}}\Big) y^* \tag{3.34}$$

$${\tau_{xx}}^* \equiv \frac{\tau_{xx}}{3\eta\bar{u}/h} = 6De\Big(\frac{\bar{u}_N}{\bar{u}}\Big)^2 y^{*2} \tag{3.35}$$

To test the validity of the analytical work described above, simulations were carried out in the same channel as it was for the Newtonian case. The properties of the fluid were the same as the test cases C, D and E reported in the work of Peres et al. [4], except that the ξ parameter of the PTT model used was set to zero. Given the fact that the *Reynolds* and *Deborah* numbers are calculated based on the half-width of the channel, and not the hydraulic diameter, the velocity and the relaxation time of the fluid had to be adjusted. The properties used are summarized in table 3.4.

Table 3.4: Properties simulated for SPTT channel flow

Property	Value	Unit
ρ	1000	[W/m^2]
η	0.1155	[Pa.s]
C	418	[J/KgK]
λ	0.375	[s]
k	0.61	[W/mK]
$\bar{u}$	0.8	[m/s]
ε	0.25	[-]

The simulated *Reynolds* number was of 31.17, the *Deborah* number was of 66.67, and given the fact that the thermal properties were to be considered equal to those of water (C≈4180 J/KgK), the specific heat was reduced to one tenth of his value, thus $C = 418$ J/KgK, and the *Prandtl* number was of 79.15, to ensure that the flow would attain fully developed conditions. The results for the comparison made for numerical results with the analytical results are described in figures 3.7, 3.8 and 3.9, for the velocity, shear stress and normal stress profiles, respectively.

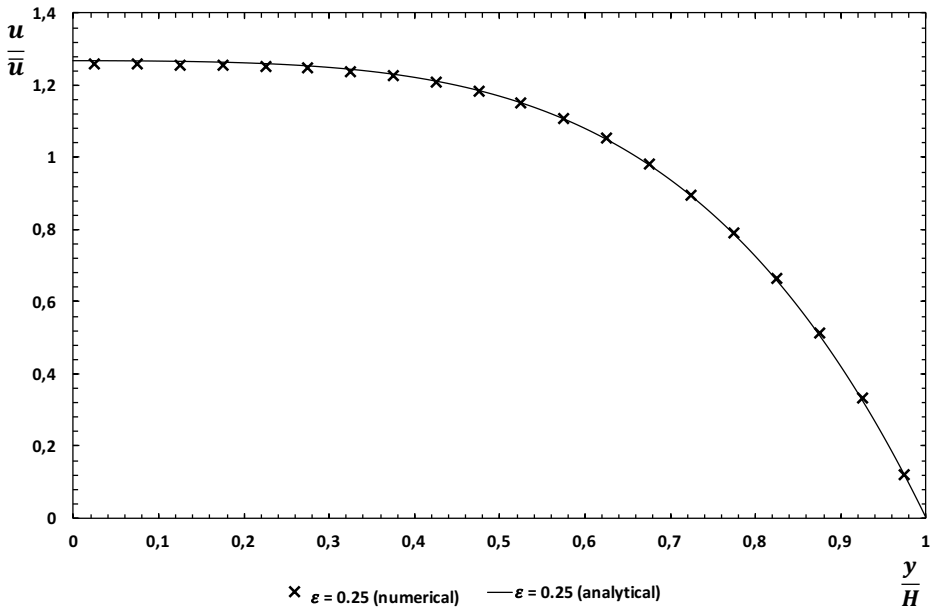

Figure 3.7: Analytical and numerical values for the velocity profile, for SPTT fluid flow, $\varepsilon = 0.25$, $De = 66.67$.

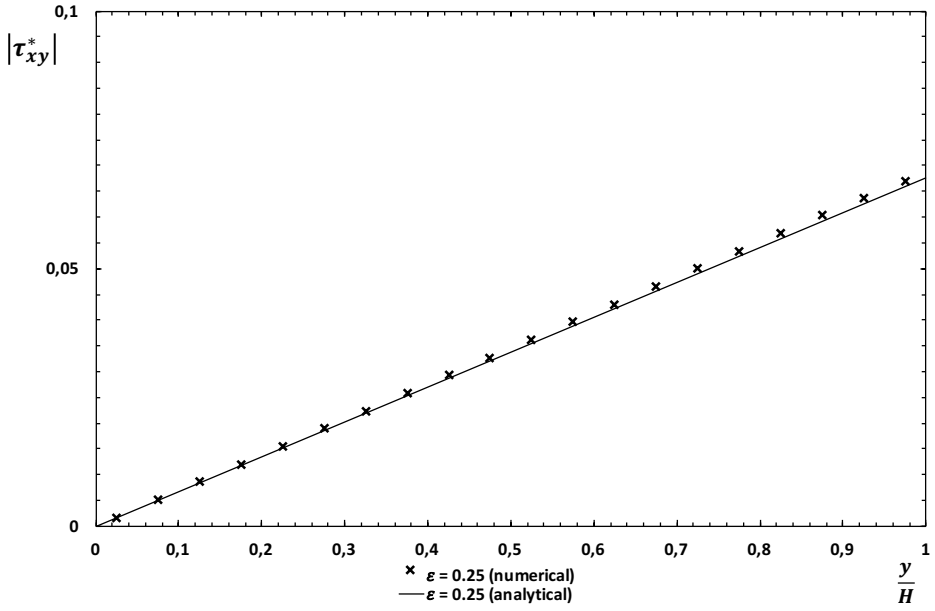

Figure 3.8: Analytical and numerical values for the shear stress profile, for SPTT fluid flow, $\varepsilon = 0.25$, $De = 66.67$.

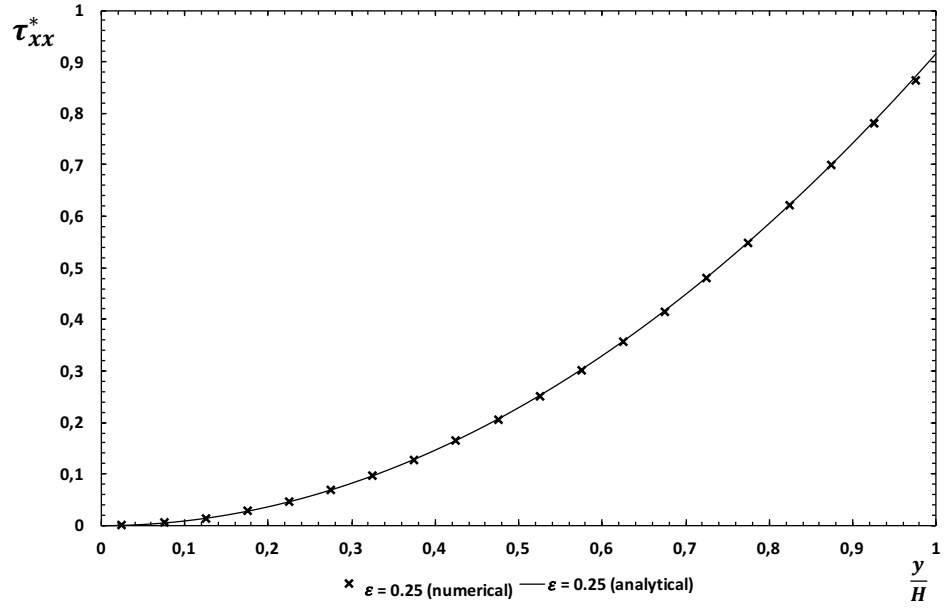

Figure 3.9: Analytical and numerical values for the normal stress profile, for SPTT fluid flow, $\varepsilon = 0.25$, $De = 66.67$.

The solution for the heat transfer problem was also obtained by Pinho and Oliveira [34], which takes into account the hydrodynamic solution described in Oliveira and Pinho [47], but the parameter b described in equation (3.30) is modified, for the case of channel flow, now called a, equation (3.36).

$$a = 9\varepsilon De^2 \left(\frac{\bar{u_N}}{\bar{u}}\right)^2 \tag{3.36}$$

The temperature distribution is as follows in equation (3.37),

$$T(y) - T_c = \frac{\rho C}{k} \frac{3\bar{u_N} h^2}{2} \frac{\partial T}{\partial x} \left(\frac{1+a}{2} \left(\frac{y}{h}\right)^2 - \frac{1}{12} \left(\frac{y}{h}\right)^4 - \frac{a}{30} \left(\frac{y}{h}\right)^6 \right) \tag{3.37}$$

where T_c is the centerline temperature of the channel, and is related to the average temperature of the flow, equation (2.8), and $\bar{T}$ is related with the wall heat flux by means of equation (2.7). The wall temperature can be obtained by setting $y = h$, equation (3.38),

$$T_w - T_c = \frac{\rho C}{k} \frac{3\bar{u_N} h^2}{4} \frac{\partial T}{\partial x} \left(\frac{5}{6} + \frac{14}{15} a \right) \tag{3.38}$$

and by making use of equation (2.8), we arrive at equation (3.39), thus defining the average temperature of the flow.

$$\bar{T} - T_c = \frac{\frac{\rho C}{k} \frac{9\bar{u_N} h^2}{20} \frac{\partial T}{\partial x} \left(\frac{108}{231} a^2 + \frac{145}{189} a + \frac{13}{42} \right)}{1 + \frac{6}{5} a} \tag{3.39}$$

Making use of the normalization made in equation (3.23) for the Newtonian case, the temperature distribution assumes the form of equation (3.40).

$$\theta(y) = \frac{-\left(1+\frac{6}{5}a\right)\left(\frac{1+a}{2}\left(\frac{y}{h}\right)^2 - \frac{1}{12}\left(\frac{y}{h}\right)^4 - \frac{a}{30}\left(\frac{y}{h}\right)^6 + -\frac{5}{12} - \frac{7}{15}a\right)}{\frac{808}{1925}a^2 + \frac{232}{315}a + \frac{102}{315}} \tag{3.40}$$

Once more, Newton's law of convection (equation 2.7) provides the heat transfer coefficient of the flow. And proceeding with the normalization, the *Nusselt* number for channel flow of the SPTT fluid with an imposed heat flux on the wall is as described in equation (3.41).

$$Nu = \frac{4}{\frac{1212}{1925}a^2 + \frac{116}{105}a + \frac{17}{35}} \tag{3.41}$$

Figure 3.10 shows the comparison made between the numerical and analytical values for the temperature profile for the SPTT fluid, with $\varepsilon = 0.25$. For the axial *Nusselt* number, its tendency is described in figure 3.11.

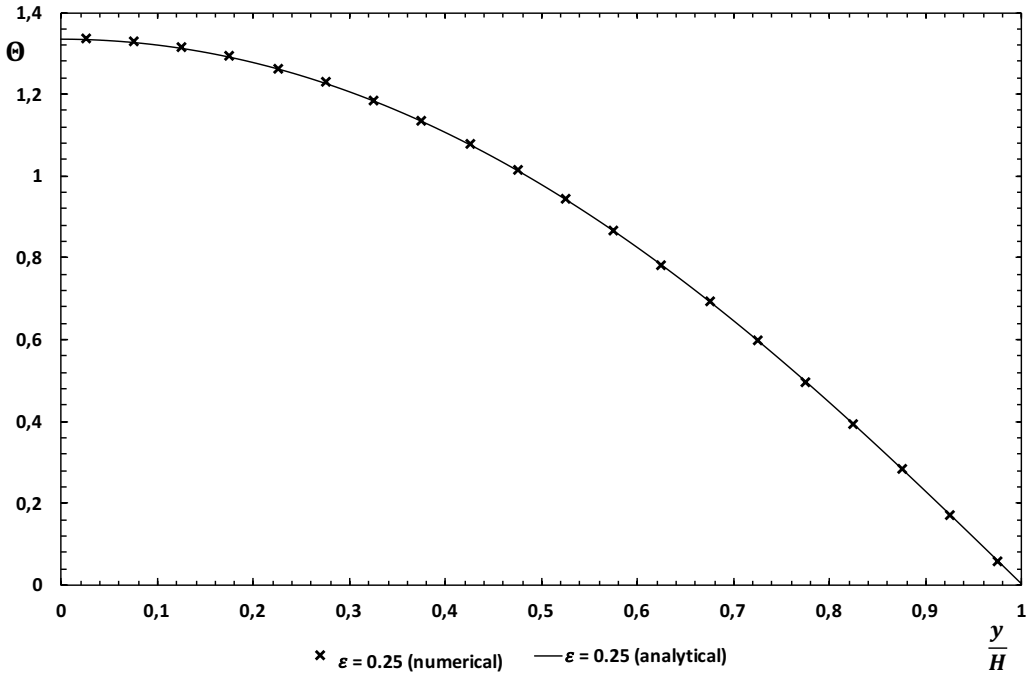

Figure 3.10: Analytical and numerical values for the temperature profile, for SPTT fluid flow, $\varepsilon = 0.25$, $De = 66.67$.

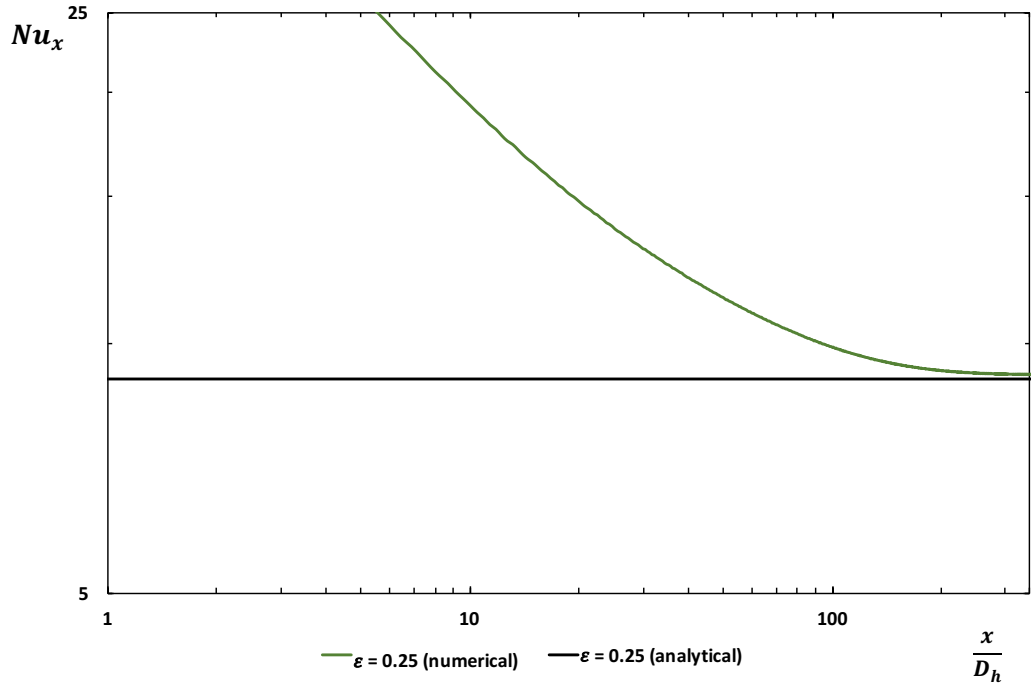

Figure 3.11: Asymptotic tendency for the Nusselt number to the corresponding analytical value, for fully developed conditions, along the axial direction of the channel, $\varepsilon = 0.25$, $De = 66.67$.

3.3.2.3 Full Phan-Thien and and Tanner fluid in channel flow

We take upon the analytical solution developed by Alves et al [48], wich is an extent of the work carried out by Oliveira and Pinho [47], but with the assumption of non-zero second normal stress difference, $\xi \neq 0$. And for the presented solution, the linearized form of the specific function of the PTT model was used, equation (2.5). The solution does not take into account the presence of a Newtonian solvent, so $\eta_p = \eta$, and $\beta_s = 0$.

Due to the extent and complexity of the solutions, the final results for the analytical solutions will be presented here, and more detailed information on the solution of the problem can be consulted in reference [48]. The variation of the shear stress is shown to be independent of the constitutive relation adopted for the stresses, according to the momentum equation, so its form is the same as it was presented in sections 3.3.2.1 and 3.3.2.2. The normal stress τ_{xx} is given by equation (3.42),

$$\tau_{xx} = \frac{\eta}{2\lambda\xi}\left(1 - \sqrt{1 - (a\frac{y}{h})^2}\right) \tag{3.42}$$

where a is a parameter introduced for compactness, given by equation (3.43),

$$a = 6\frac{\bar{u_N}}{\bar{u}} De\sqrt{\varepsilon\,(1-\xi)}\sqrt{\chi} \tag{3.43}$$

and χ is a second compactness parameter that combines the two parameters of the PTT model, as shown in equation 3.44.

$$\chi \equiv \frac{\xi\,(2-\xi)}{\varepsilon\,(1-\xi)} \tag{3.44}$$

It was shown by Alves et al. [48] that τ_{xx} and τ_{yy} are related by the ξ parameter of the PTT model, thus resulting in equation (3.45) for the τ_{yy} profile.

$$\tau_{yy} = \frac{\eta}{4\lambda\,(2-\xi)}\left(1-\sqrt{1-(a\frac{y}{h})^2}\right) \tag{3.45}$$

The velocity profile of the flow, in fully developed conditions, is given by equation (3.46).

$$\begin{gathered} u(y) = \frac{2\eta}{\lambda^2\xi\,(2-\xi)\left(\frac{\partial p}{\partial x}\right)}\left[1+\frac{2}{\chi}\right] \\ \times\left[\ln\left(\frac{1-\sqrt{1-(a\frac{y}{h})^2}}{1-\sqrt{1-a^2}}\right)+\sqrt{1-a^2}-\sqrt{1-(a\frac{y}{h})^2}\right] \\ +\frac{\frac{\partial p}{\partial x}h^2}{\eta\chi}\left(1-\left(\frac{y}{h}\right)^2\right) \end{gathered} \tag{3.46}$$

The normalized form of the stresses are obtained by scaling the with the wall shear stress for a Newtonian fluid, as it was made for the case of the SPTT fluid. In non-dimensional form, the stresses are as follows in equations (3.47), (3.48) and (3.49) for τ_{xx}, τ_{yy} and τ_{xy}.

$${\tau_{xx}}^* \equiv \frac{\tau_{xx}}{3\eta\bar{u}/h} = \frac{1-\sqrt{1-(a\frac{y}{h})^2}}{6De\xi} \tag{3.47}$$

$${\tau_{yy}}^* \equiv \frac{\tau_{yy}}{3\eta\bar{u}/h} = -\frac{1-\sqrt{1-(a\frac{y}{h})^2}}{6De\,(2-\xi)} \tag{3.48}$$

$${\tau_{yy}}^* \equiv \frac{\tau_{xy}}{3\eta\bar{u}/h} = -\frac{a\frac{y}{h}}{6De\sqrt{\xi\,(2-\xi)}} \tag{3.49}$$

For the profile velocity, its normalized form is obtained by scaling with the average velocity $\bar{u}$, equation (3.50),

$$\begin{gathered} \frac{u(y)}{\bar{u}} = -\frac{6}{a^2}\frac{\bar{u}_N}{\bar{u}}\left[1+\frac{2}{\chi}\right] \\ \times\left[\ln\left(\frac{1-\sqrt{1-(a\frac{y}{h})^2}}{1-\sqrt{1-a^2}}\right)+\sqrt{1-a^2}-\sqrt{1-(a\frac{y}{h})^2}\right] \\ -\frac{3}{\chi}\frac{\bar{u}_N}{\bar{u}}\left[1-\frac{y}{h}^2\right] \end{gathered} \tag{3.50}$$

and the integration of the normalized velocity profile, using the definition presented by equation (3.15), provides calculation for the ratio $\frac{\bar{u}_N}{\bar{u}}$, equation (3.51).

$$\left(\frac{\bar{u}_N}{\bar{u}}\right)^{-1} = \frac{6}{a^2}\left[1+\frac{2}{\chi}\right]\left(1-\frac{\pi}{4a}+\frac{1}{2a}\arctan\left(\frac{\sqrt{1-a^2}}{a}\right)-\frac{\sqrt{1-a^2}}{2}\right)-\frac{2}{\chi} \tag{3.51}$$

Equation (3.51) does not provide an explicit expression for the ratio $\frac{\bar{u}_N}{\bar{u}}$, however. Equation (3.51) must be solved together with equation (3.43) by numerical means, using a straight bissection method [48].

Inspection of the normal stress profiles (equations (3.42) and (3.45)) shows that a real solution can only be obtained if $a\frac{y}{h} \leqslant 1$. Since the normalized lateral coordinate $\frac{y}{h}$ varies from 0 to 1, then this in turn implies that $a \leqslant 1$. As shown by Alves et al. [48], $a \geqslant 1$ represents a constitutive flow instability, and real solutions to the flow can only be obtained if the following condition is respected:

$$De \leqslant De_c \iff De \leqslant \frac{1}{\sqrt{\xi\,(2-\xi)}}\left[\left(1-\frac{\pi}{4}\right)+\frac{1}{3\chi}\left(5-\frac{3}{2}\pi\right)\right] \tag{3.52}$$

The analytical solution was compared to numerical simulations of a fluid, whose properties are described as follows in table 3.5.

Table 3.5: Properties simulated for PTT channel flow, with $\xi \neq 0$

Property	Value	Unit
ρ	1000	[W/m^2]
η	0.1155	[Pa.s]
C	418	[J/KgK]
λ	0.04386	[s]
k	0.61	[W/mK]
$\bar{u}$	0.513	[m/s]
ϵ	0.25	[-]
ξ	0.01	[-]

Due to the fact that the condition imposed by (3.52) had to be respected, otherwise comparison could not be made with a real solution to the problem, the *Deborah* number was adjusted to 5, hence the difference between the average velocity and relaxation times reported in table 3.4. For the present flow conditions, the critical *Deborah* number is 35.2, so it was assured that the flow was well within the limits for obtaining a valid solution. The comparison between the analytical and numerical values is shown in figures 3.12, 3.13,3.14 and 3.15, for the velocity and stress profiles. The mesh used was the same for the simplified PTT fluid described in section 3.3.2.2.

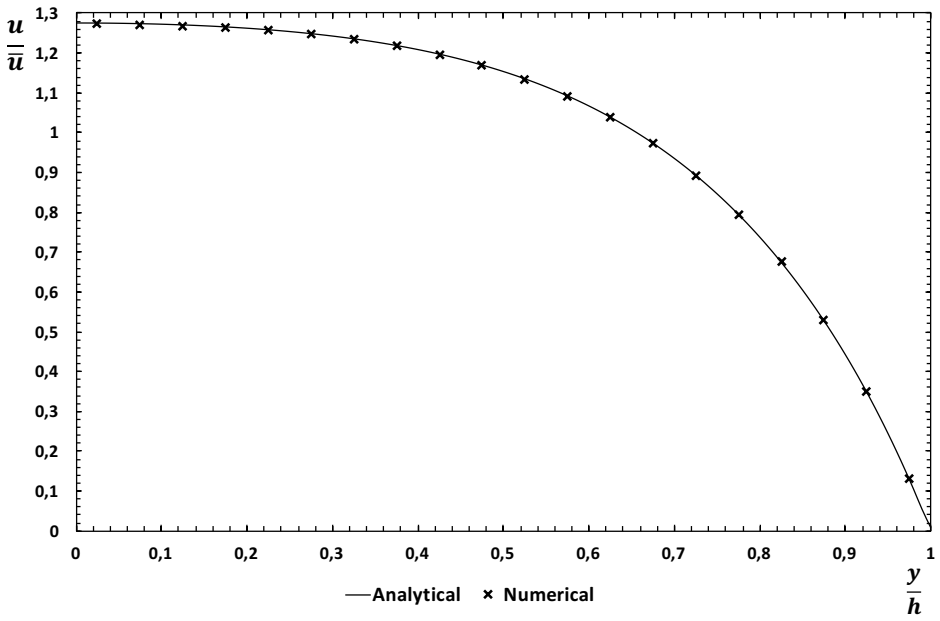

Figure 3.12: Analytical and numerical values for the velocity profile of the complete PTT model, $\varepsilon = 0.25$,$\xi = 0.01$,$De = 5$.

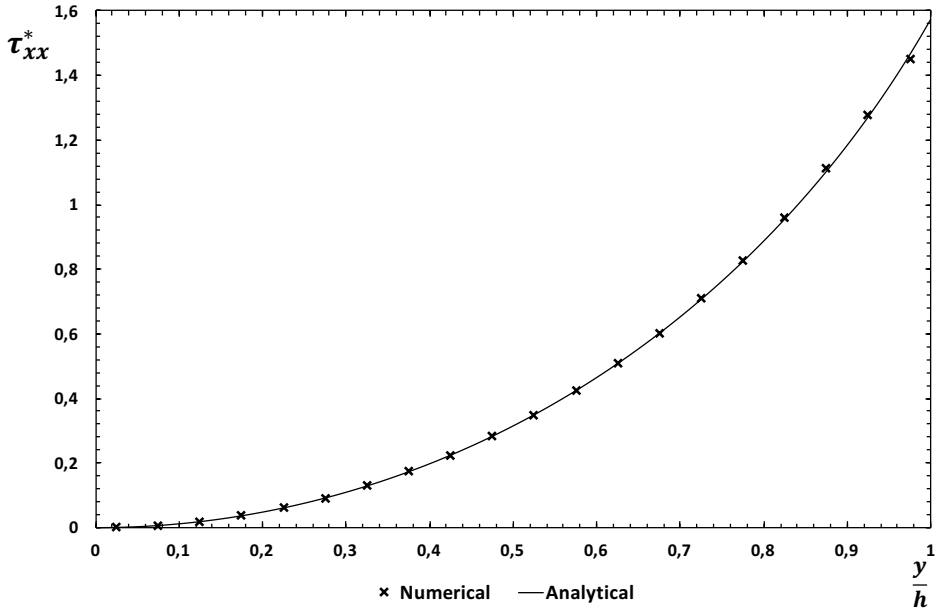

Figure 3.13: Analytical and numerical values for the normal stress τ_{xx} *of the complete PTT model,* $\varepsilon = 0.25$, $\xi = 0.01$, $De = 5$.

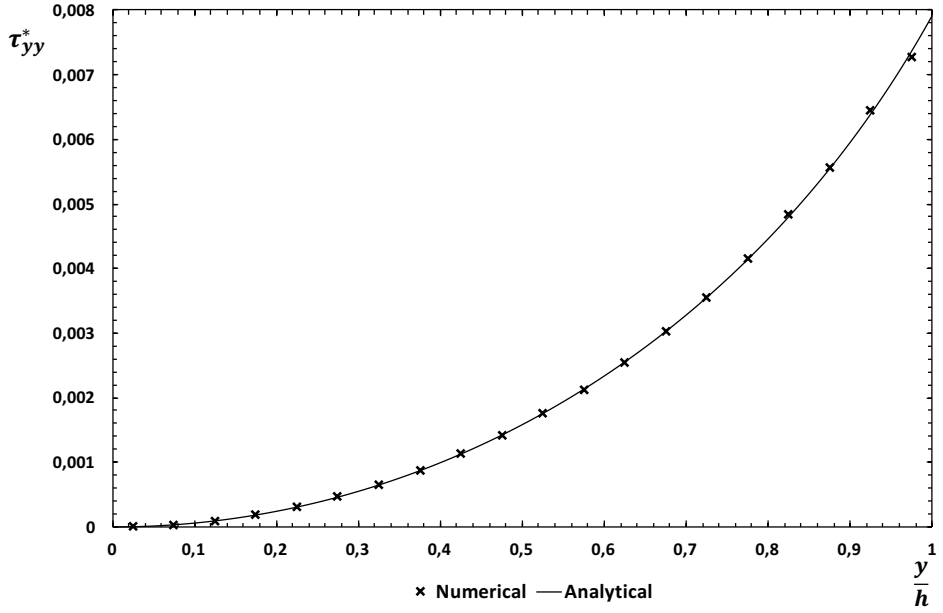

Figure 3.14: Analytical and numerical values for the normal stress τ_{yy} of the complete PTT model, $\varepsilon = 0.25$, $\xi = 0.01$, $De = 5$.

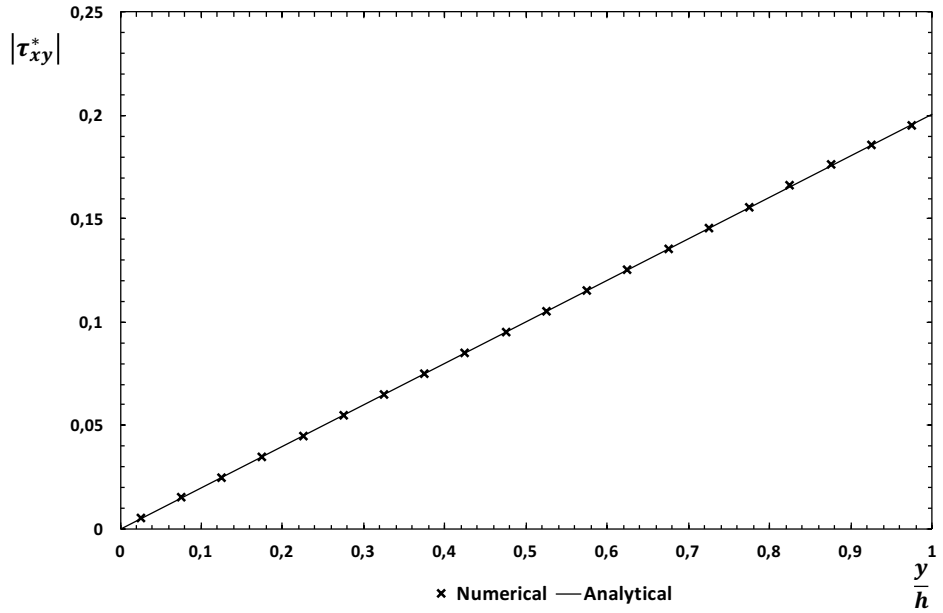

Figure 3.15: Analytical and numerical values for the shear stress τ_{xy} of the complete PTT model, $\varepsilon = 0.25$, $\xi = 0.01$, $De = 5$.

3.3.3 Newtonian duct flow

This section presents the results obtained for the heat transfer analysis carried out for a Newtonian fluid. The geometry employed was the same as the numerical works carried out in the numerical procedure reported by Peres et al. [4], and the experimental work carried by Hartnett and Kostic [28], except the length L of the duct was cut to half the size reported in both papers. The length adopted in the referred papers was of 6.4 meters, and in the present simulations the length was of 3.2 m.

Two different conditions were simulated. A case where all walls were heated, and a case where only the upper and lower walls were heated, as considered in references [28] and [4]. The aspect ratio of the duct simulated in the referenced papers was of 2, but in this present work it is also included the comparison for a duct with an aspect ratio of 1.

The numerical results were compared with the analytical values listed in Shah and London [42], for fully developed flow conditions. Figure 3.16 shows the variation of the axial *Nusselt* number for the duct with the aspect ratio of 1, compared with the analytical solution [42].

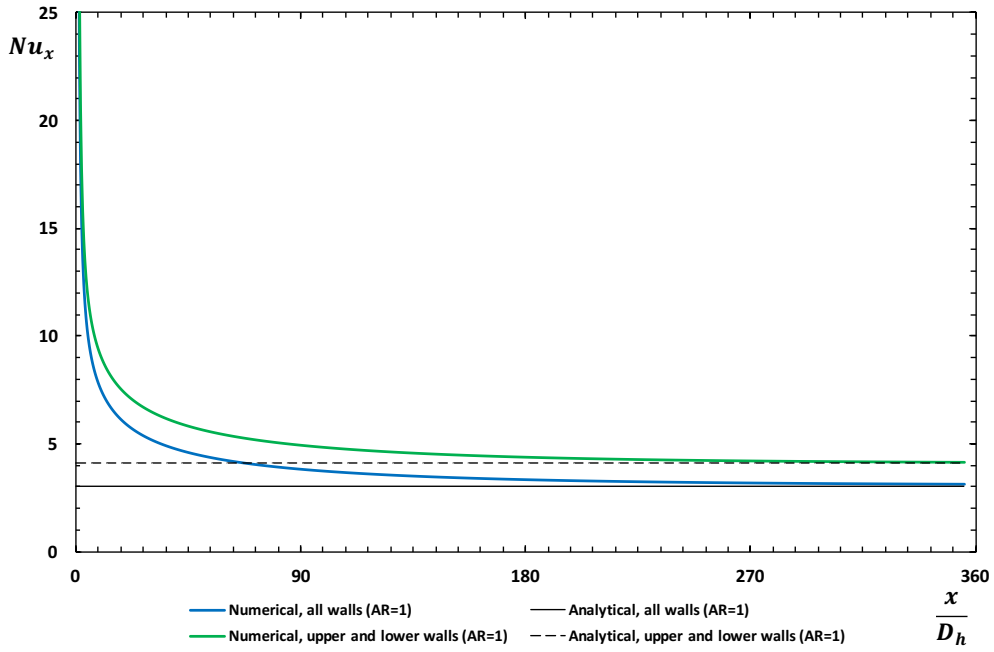

Figure 3.16: Asymptotic tendency for the Nusselt number to the corresponding analytical value, for fully developed conditions, along the axial direction of the duct. Newtonian fluid flowing in a duct with $AR = 1$.

Figure 3.17 presents the numerical results for the case of the duct with an aspect ratio of 2, also comparing with the analytical values extracted from [42].

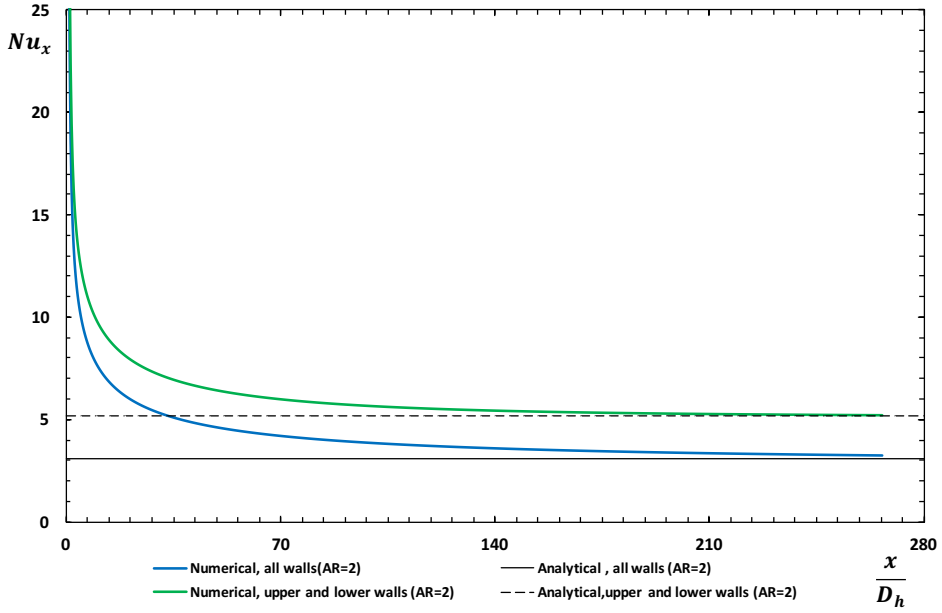

Figure 3.17: Asymptotic tendency for the Nusselt number to the corresponding analytical value, for fully developed conditions, along the axial direction of the duct. Newtonian fluid flowing in a duct with $AR = 2$.

3.3.4 Discussion of results

Simulations were carried out for channel flow, and duct flow with two different aspect ratios, 1 and 2. For the case of channel flow, the velocity, temperature and stress profiles were compared, whereas for 3D flow, analysis was made on the *Nusselt* of the flow. The results obtained are in good agreement with the ones present in literature.

For Newtonian flow in a channel, analytical solutions exist for the velocity, shear stress and temperature profiles. The obtained numerical profiles for the velocity and shear stress provided quite good results when compared to the analytical curves. The error for the velocity ranged from values between 0.51% and 1.79%. In the case of the shear stress profile, the error was constant for all the numerical values, of 0.76%. For the temperature profile, the minimim and maximum deviations from the analytical solution were of 0.87% and 2.99%,respectively.

The analytical *Nusselt* number for fully developed channel flow is of 8.235, according to Shah and London [42], and the numerical result was of 8.3024, a difference of 0.82%. There is also a disturbance observed at the end of the channel, and was only observed in this present case. Checking the errors in that disturbance, it can be observed that *Nusselt* oscillates between two different values, one of 8.2348 and another 8.3317, which means the error in that zone can be ranged from 0.0024% to 1.1743%.

In the case of SPTT fluid flow in a channel, the analytical solution for the stress and velocity profiles was extracted from Oliveira and Pinho [47]. The analytical solution for the thermal quantities was extracted from work carried out by

the same authors [34]. For the velocity profile, the difference between the numerical and analytical values ranged from a minimum of 0.68% to a maximum of 3.65%. The numerical values for the shear stress present a difference from the analytical curves with values ranging from 1.52% to 1.73%. The normal stress τ_{xx} presents great improvement, with errors ranging from 0.51% to 0.92%. In the case of the temperature profile, the difference reported was between the limits of 0.23% and 0.4%.

Since the *Nusselt* number shows dependency on the ε parameter of the PTT model (equation 3.41), its variation was plotted and simulations were carried out by simply varying the ε parameter, for values of 0.01, 0.05, 0.1, 0.15, 0.2 and the simulation for $\varepsilon = 0.25$ was also included in figure 3.18.

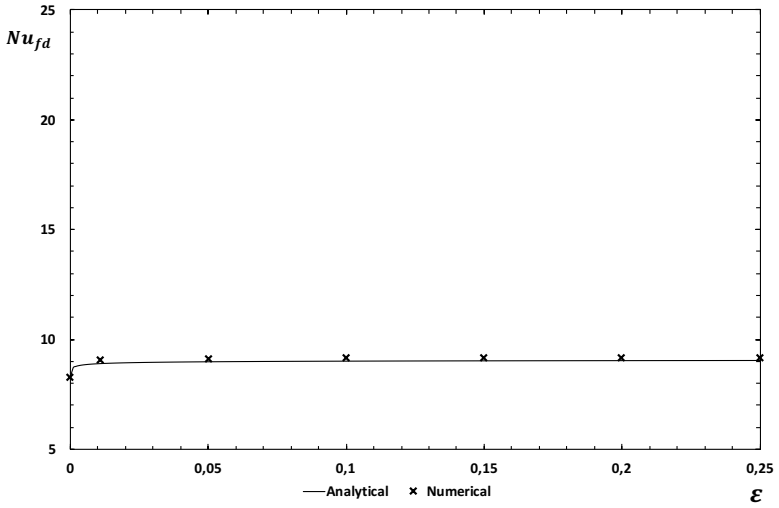

Figure 3.18: Variation of Nusselt number with the ϵ parameter of the PTT model. fd stands for fully developed.

As can be seen in this plot, the numerical values for the fully developed *Nusselt* exhibit the same behavior as the ones predicted in literature. The maximum difference observed was of 1.96%, for $\varepsilon = 0.01$. As the ε parameter is increased, the error for the predicted *Nusselt* number decreases. For the maximum value of $\varepsilon = 0.25$, the error is of 1.23%.

To test the influence of the ξ parameter on the numerical runs, simulations were carried out for the complete PTT model, and the obtained numerical values were compared with the analytical solution presented by Alves et al [48]. Since there is no known thermal solution for the PTT model with $\xi \neq 0$, only the dynamic quantities were compared. The velocity field presents a deviation from the analytical curve, with error values ranging from 0.18% to 1.33%. The agreement with predicted analytical curves for the normal stresses τ_{xx} and τ_{yy} is also excellent. In the case of τ_{xx}, the error ranges from 0.42% to 1.33%. The τ_{yy} profile presents a deviation from the analytical function with errors limited between 0.91% and 1.37%. The shear stress presents the most accurate fitting, with an error comprehended between 0.21% and 0.37%.

Because no known solution for the fluid dynamics and heat transfer of the PTT model exists, in the case of three dimensional flow, the only means of testing the accuracy of the 3D mesh employed was by comparing the *Nusselt* number for a Newtonian case.

For the heat transfer analysis, simulations were carried out for two different boundary cases. In the first trial, all walls were heated and the analytical values for the *Nusselt* is of 3.02 and 3.092, for AR of 1 and 2, respectively [42]. The numerical values for the corresponding *Nusselt* is of 3.15 for $AR = 1$, registering an error of 4.3%. For $AR = 2$, the numerical value for the *Nusselt* number was of 3.25, thus marking a difference of 5.1%.

In the case where only the upper and lower walls are heated (the side walls are considered adiabatic), the *Nusselt* values available in literature are of 4.094 and 5.2, for for AR of 1 and 2, respectively [42]. For $AR = 1$, the extracted *Nusselt* was of 4.14, showing a deviation of 1%. In the case of $AR = 2$, the numerical *Nusselt* was of 5.18, marking a difference of 0.4%.

Due to the large computational time needed for the 3D simulations to achieve convergence, it was only possible to simulate ducts with an aspect ratio of 2. The boundary condition where only the upper and lower walls are heated was chosen, because it presented the smallest deviation from the analytical values observed in literature. For the more complex viscoelastic models ($\xi \neq 0$), most of the simulations present in this work, for three-dimensional meshes could take weeks before convergence was achieved. Because of this limitation, the simulations carried in chapter 4 were employed using only mesh B, defined in table 3.2, which provided the fastest simulations times, and showed good results for the heat transfer coefficient.

Chapter 4

Numerical results

This chapter presents the results obtained. In this work, the simulations were carried out in mesh DB, which has half the length L of mesh DA. The first trials were carried out in mesh DA, with the same parameters described for models C, D and E reported in the numerical work carried out by Peres et al. [4]. As reported in their work, apart from the viscosity, the other thermophysical properties (density ρ, specific heat C and thermal conductivity k) were assumed the same as water. Table 4.1 presents a summary of the flow conditions imposed on the simulations carried out by Peres et al. [4].

Table 4.1: Properties adopted for PTT duct flow in the work by Peres et al. [4]

Property	Value	Unit
ρ	1000	[W/m^2]
η_p	0.11	[Pa.s]
η_s	0.0055	[Pa.s]
C	4180	[J/KgK]
λ	0.5	[s]
k	0.61	[W/mK]
$\bar{u}$	0.8	[m/s]
ε	0.25	[-]
ξ	0.01 to 0.03	[-]

The simulated *Reynolds* and *Deborah* numbers, based on the hydraulic diameter, were of 83.12 and 33.33. As the specific heat and thermal conductivity were assumed the same as water, the simulated *Prandtl* number was of 791.46. The mesh used by Peres et al [4] was the same mesh used to reproduce the results reported in their paper, mesh DA (table 3.2).

The mesh used for the results presented in section 4.2 was mesh DB, defined in table 3.2, equivalent to mesh DA, except for the length L, which was cut to half ($L = 3.2$ m). To ensure minimization of the dynamic and thermal entrance length of the fluid in the duct, the results obtained in this work were simulated for a smaller *Reynolds* number ($Re = 20$), and a *Prandtl* of a quarter of the Pr defined in the previous paragraph ($Pr = 197.87$). To achieve these values, the average velocity and specific heat were adjusted. The parameters are summarized in table 4.2.

Table 4.2: Properties adopted in the simulations carried out in the present work

Property	Value	Unit
ρ	1000	[W/m^2]
η_0	0.1155	[Pa.s]
C	1045	[J/KgK]
k	0.61	[W/mK]
$\bar{u}$	0.1925	[m/s]
ε	0.25	[-]
ξ	0 to 0.05	[-]

4.1 Increase of secondary flow in the fluid

This section starts with a summary of the results obtained in mesh DA, for models C ($\xi = 0.01$), D ($\xi = 0.02$) and E ($\xi = 0.03$) of the work by Peres et al [4]. In addition, flow conditions for the simplified version of the PTT model were simulated ($\xi = 0$), to quantify the gap between the existence of secondary flow arising in the fluid, comparing to the case where $N_2 = 0$ (no secondary flow). The results are shown in figure 4.1.

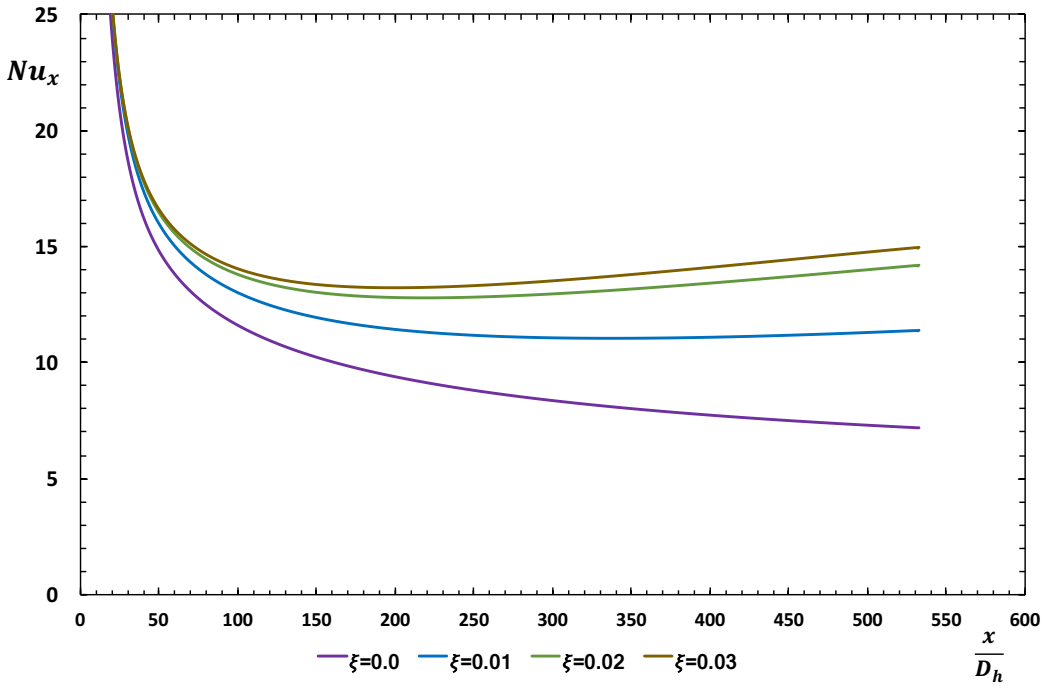

Figure 4.1: Effects of the increase of secondary flow in the heat transfer of the fluid. $Re = 83.12$, $De = 33.33$, $\varepsilon = 0.25$

As can be seen by the results obtained, if no secondary flow is considered ($\xi = 0$), the *Nusselt* number tends to an asymptotic behavior similar to what was observed in Newtonian fluid flow. However, if the model predicts a non-zero second normal stress coefficient ($\xi \neq 0$), the asymptotic behavior is reversed. In fact, even for the fluid with the lowest ξ parameter, 0.01, a slight increase in Nu was registered. It would appear that secondary flow has a strong impact on the thermal entrance length of the flow. For the SPTT fluid ($\xi = 0$) the increase in the *Nusselt* number, in comparison with a Newtonian fluid, is of 39 %.

4.1.1 Influence of ε on the PTT model

To test the influence of the ε parameter on the models simulated by Peres et al [4], additional simulations were carried out by testing values of ε of 0.1, 0.15 and 0.2. The results for the heat transfer behavior are summarized in figure 4.2.

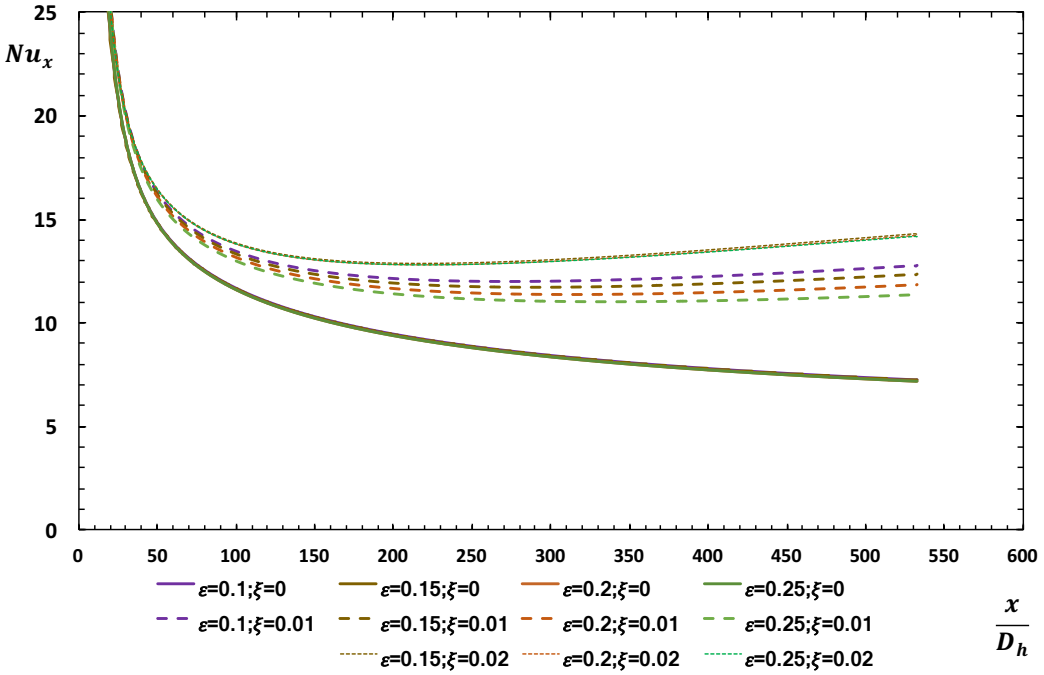

Figure 4.2: Effects of ε on the PTT model, either in simplified form ($\xi = 0$) and in the complete version ($\xi \neq 0$). $Re = 83.12$, $De = 33.33$.

From figure 4.2, it can be observed that, in the absence of secondary flow, ε does not affect the heat transfer behavior of the fluid. The same cannot be said for the cases where $\xi \neq 0$. It would appear that these parameters influence each other. In fact, if ξ increases the heat transfer coefficient of the fluid, ε has the reverse effect. It seems that, the increase of the shear-thinning behavior of the fluid has a negative impact on the transverse velocities, thus diminishing the intensity of secondary flow, thereby decreasing the heat transfer coefficient of the fluid.

This appears to be truth up to a certain point. It seems that by increasing the magnitude of secondary flow, the effects of the elongational behavior are strongly minimized. The negative effect of the ε parameter on the heat transfer behavior still shows, as can be seen by zooming figure 4.2, figure 4.3.

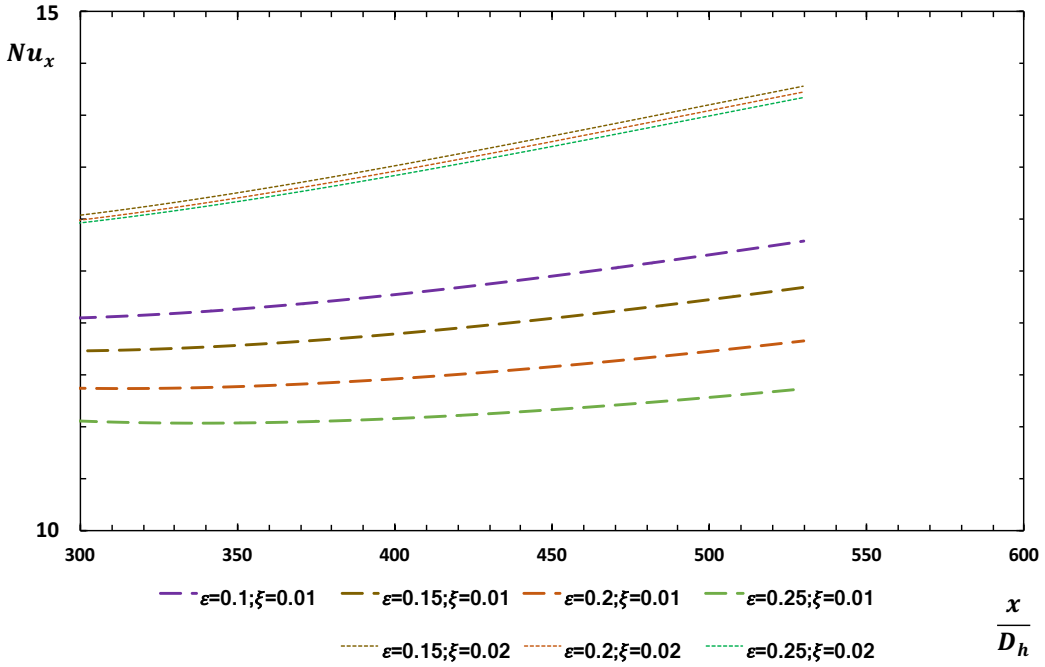

Figure 4.3: Effects of ε on the PTT model, for $\xi \neq 0$. $Re = 83.12$, $De = 33.33$.

Unfortunately, the behavior of the fluid E ($\xi = 0.03$), for different values of ε, could not be ascertained, because convergence of the simulations could not be achieved for those models. It cannot be concluded that the influence of ε in the fluid will remain the same, for bigger values of ξ. Apparently, if $\xi \neq 0$, variation of the elongational parameter of the PTT model has almost no influence on the heat transfer of the fluid, except if the secondary flow is weak.

4.2 Tests on elasticity, secondary flow, and solvent contribution

According to the results obtained in section 4.1, it seems that the chosen *Reynolds* and *Prandtl* parameters are not higher enough to enable the flow to achieve fully developed conditions for that given length of the duct. As tested in section 3.3.3, the use of mesh DB to simulate the flow behavior of a Newtonian fluid undergoing wall heating, provided very good results for the dynamic and thermal quantities of the fluid, showing a 0.4% deviation to the predicted analytical Nu, for the case where the upper and lower walls of the duct were heated, and considering adiabatic side walls.

As reported in the previous section, the influence of the ε parameter appears to have a very weak impact on the heat transfer coefficient of the fluid. Because the simulation times appear to be proportional to decreasing values of ϵ, the highest value of $\varepsilon = 0.25$ was chosen, since it provided fastest convergence. The fluid was tested for the influence of elasticity (increasing De), inclusion of a Newtonian solvent (increasing β_s), and rise of the magnitude of secondary flow (increasing ξ). The following sections present a summary of the results obtained.

4.2.1 Effect of the *Deborah* number

To test the influence of elasticity in the fluid, the effect of the relaxation time was studied. β_s and ξ were set to zero, to ensure that the effects on the heat transfer of the fluid were solely due to the variation of the *Deborah* number. Table 4.3 presents a summary of the relaxation times employed in the simulations.

Table 4.3: Relaxation times simulated in the present work

De	λ [s]
10	0.6234
20	1.2468
100	6.234
200	12.468

The resulting variation of the *Nusselt* number across the axial distance of the duct was extracted from the simulations, and the results are given in figure 4.4.

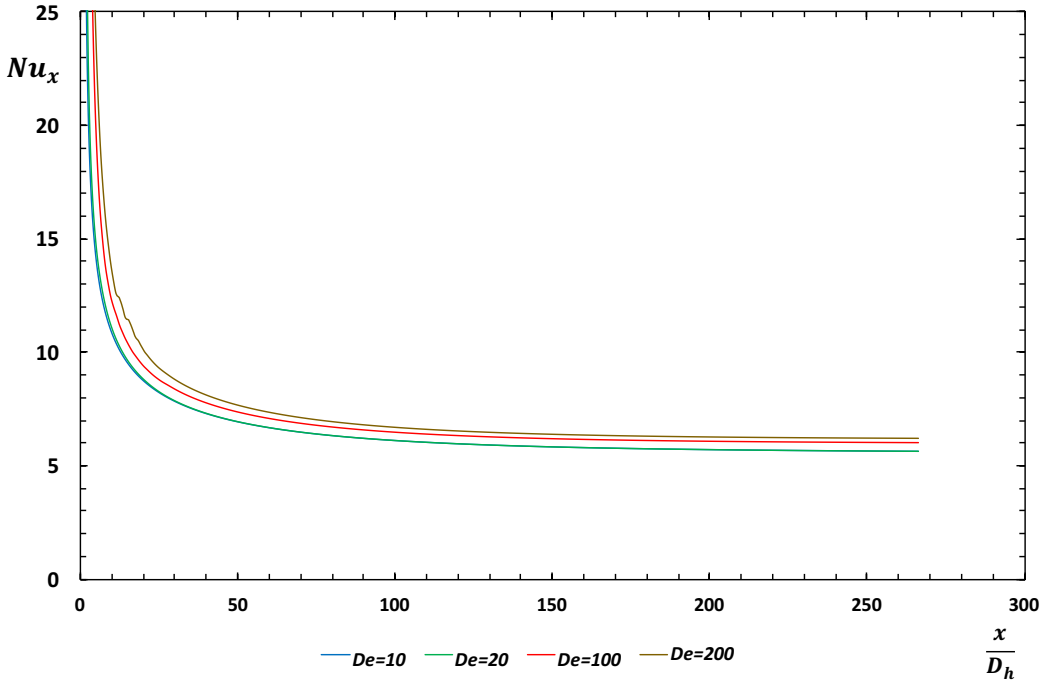

Figure 4.4: Effects of the variation of De on the tested viscoelastic runs. Test cases where the ξ parameter is zero. $\varepsilon = 0.25$.

Figure 4.4 shows that elasticity of the fluid has a positive influence on the heat transfer of the fluid. Also, it would appear that the choice of non-dimensional parameters for these trial runs allowed the visualization of fully developed thermal conditions, as opposed to what was observed by Peres et al. [4]. Apparently, for small values of De, it would appear that predicted numerical Nu for fully developed conditions comes close to the reported Newtonian solution.

Figure 4.5 presents a magnification of figure 4.4, in order to better visualize the difference between the fully developed *Nusselt* numbers registered, with the inclusion of the Newtonian case.

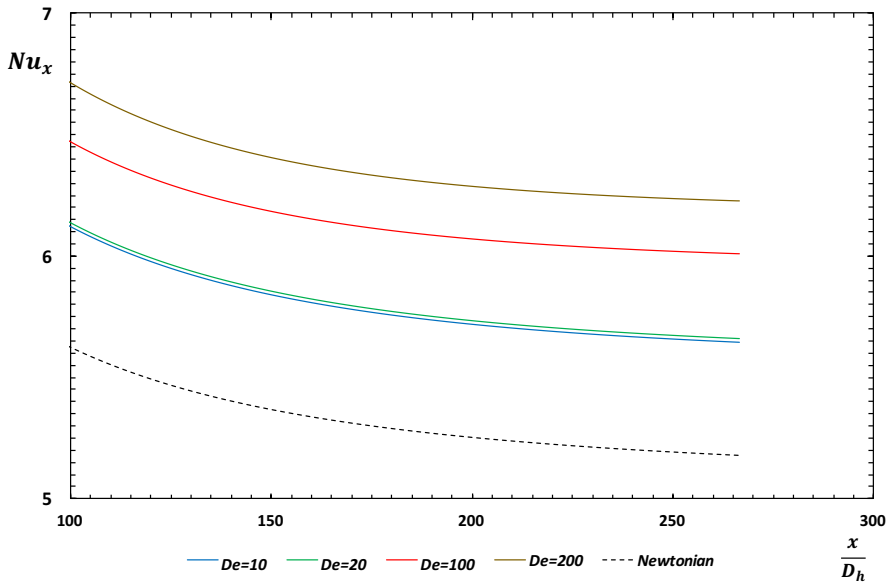

Figure 4.5: Fully developed behavior of Nu, for different Deborah numbers ($\varepsilon = 0.25$). Comparison with the Newtonian case is included.

The increase of the relaxation time of the fluid enhances the heat transfer coefficient, comparing to the Newtonian case. For small values of De, the difference between the heat transfer coefficient for values of $De = 10$ and $De = 20$ is small, about 0.3%, whereas for the curves pertaining $De = 100$ and $De = 200$, the difference between both is of 3.63%. It would appear the bigger the elasticity of the fluid, the higher the heat transfer coefficient of the fluid will be, as expected, but it would appear that the increase is not linear. In fact, the increase from setting $De = 100$, comparing with $De = 10$ is of 6.44%, while the registered difference between the $De = 20$ and $De = 200$ cases is of 9.98%. As for the increase in comparison with the Newtonian case, the values are registered in table 4.4.

Table 4.4: Percentage of increase in *Nu*, by comparison to a Newtonian fluid

De	Increase (%)
10	8.96
20	9.29
100	15.97
200	20.18

4.2.2 Effect of a Newtonian solvent contribution

The contribution of the Newtonian solvent was also studied. The total viscosity η_0 was unchanged, and this was achieved by varying the proportion between the polymer viscosity η_p and the solvent viscosity η_s. The viscosities tested are described in table 4.5.

Table 4.5: Polymer and Newtonian viscosities employed in the trial runs.

β_s	η_p [Pa.s]	η_s [Pa.s]
0	0.1155	0
0.25	0.086625	0.028875
0.5	0.05775	0.05775
0.75	0.028875	0.086625

The different values of β_s were tested for the SPTT fluid ($\xi = 0$), in order to establish the total difference to the heat transfer coefficient in the models described in section 4.2.1. The increase in β_s was then tested for the different *Deborah* values described in the previous runs.

4.2.2.1 *De*=10

Figure 4.6 shows the influence of the Newtonian solvent in the flow, for the case where $De = 10$ and $\xi = 0$.

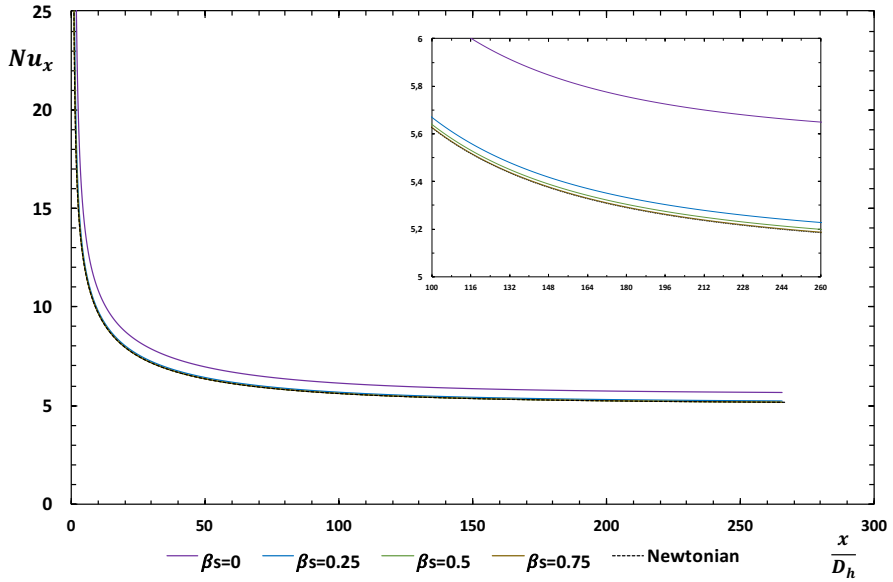

Figure 4.6: Contribution of the Newtonian solvent to the viscoelastic fluid. $De = 10$, $\varepsilon = 0.25$, $\xi = 0$.

As expected, the viscous contribution of the Newtonian solvent diminishes the heat transfer coefficient. The effects of adding even a small portion of Newtonian liquid ($\beta_s = 0.25$, highly concentrated polymer solution), completely reverts the be-

havior of the fluid to the expected Newtonian *Nusselt* number.

The next part of the simulations for model with $De = 10$, was to check the influence of secondary flow ($\xi \neq 0$) combined with the effect of the solvent. The trials were carried by varying the ξ parameter from 0.01 to 0.05, with $\beta_s \neq 0$. The results are presented in figures 4.7,4.8 and 4.9, for β_s of 0.25, 0.5 and 0.75, respectively.

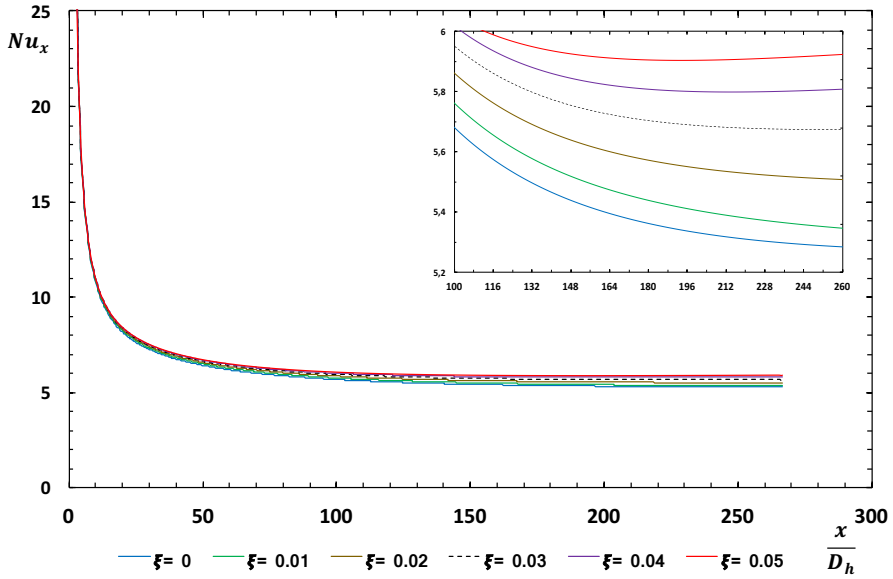

Figure 4.7: Effect of the ξ parameter on a PTT fluid, with a Newtonian solvent contribution. $De = 10$, $\varepsilon = 0.25$, $\beta_s = 0.25$.

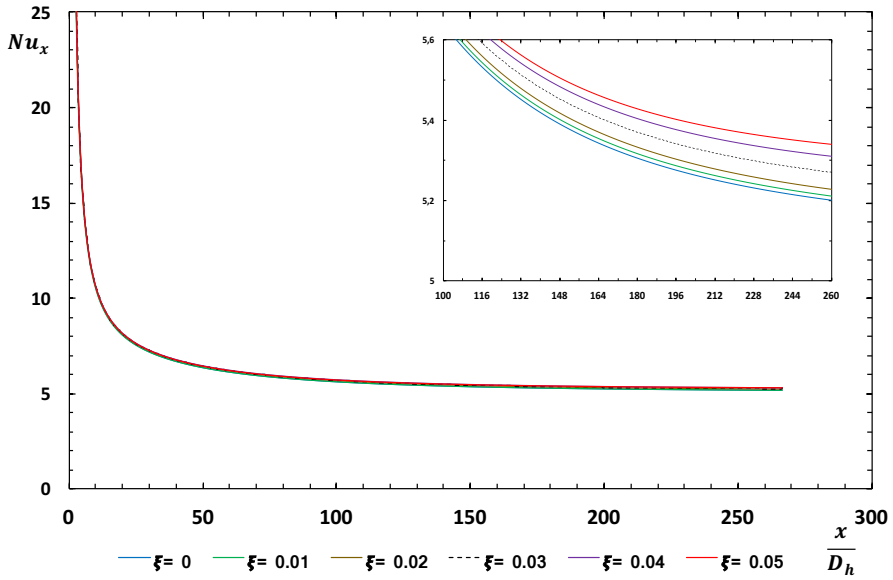

Figure 4.8: Effect of the ξ parameter on a PTT fluid, with a Newtonian solvent contribution. $De = 10$, $\varepsilon = 0.25$, $\beta_s = 0.5$.

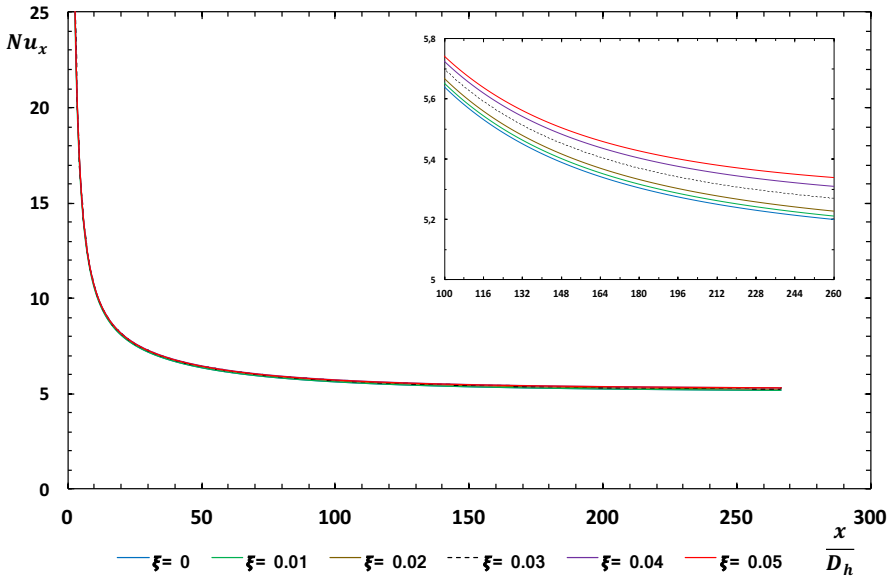

Figure 4.9: Effect of the ξ parameter on a PTT fluid, with a Newtonian solvent contribution. $De = 10$, $\varepsilon = 0.25$, $\beta_s = 0.75$.

As expected, the presence of secondary flow in the fluid causes a small enhancement in the heat transfer coefficient, even in the presence of strong quantities of Newtonian solvent (for $\beta_s = 0.75$, a highly diluted polymeric liquid). In fact, even for the case where the solution is more concentrated ($\beta_s = 0.25$), the heat transfer coefficient actually exhibits a small increase, similar the models obtained by Peres et al [4] and the ones depicted in figures 4.1 and 4.2, although the slope of the increase is much smaller (almost inexistent) in the cases pictured in figure 4.7.

By comparing the obtained values in figures 4.7, 4.8 and 4.9, with the Newtonian value for *Nu*, it can be seen a small difference to the viscoelastic simulations. The percentage of increase in *Nu* is presented in table 4.6.

Table 4.6: Percentage of increase in *Nu*, by comparison to a Newtonian fluid, $De = 10$,$\varepsilon = 0.25$

β_s	$\xi = 0.01$	$\xi = 0.02$	$\xi = 0.03$	$\xi = 0.04$	$\xi = 0.05$
0.25	3.1 %	6.1 %	9.1 %	11.6 %	13.4 %
0.5	0.85 %	1.1 %	1.6 %	2.4 %	3.1 %
0.75	0.12 %	0.33 %	0.52 %	0.65 %	0.75 %

As expected, the increase of ξ increases the heat transfer coefficient, for any quantity of Newtonian solvent in the flow. Even in the more dilute solutions ($\beta_s = 0.5$ and $\beta_s = 0.75$), the *Nusselt* is bigger than the one for Newtonian fluid, although in the case of $\beta_s = 0.75$, this difference is almost imperceptible.

4.2.2.2 De=20

The influence of the Newtonian solvent, with and without the combined effects of secondary motion in the flow, were also tested for a *Deborah* of 20. The models continue to predict the same behavior observed in section 4.2.2.1, although the influence of ξ now appears to be less accentuated than in the previous trial simulations.

Figure 4.10 presents the influence of the newtonian solvent, for the case where $De = 20$ and $\xi = 0$.

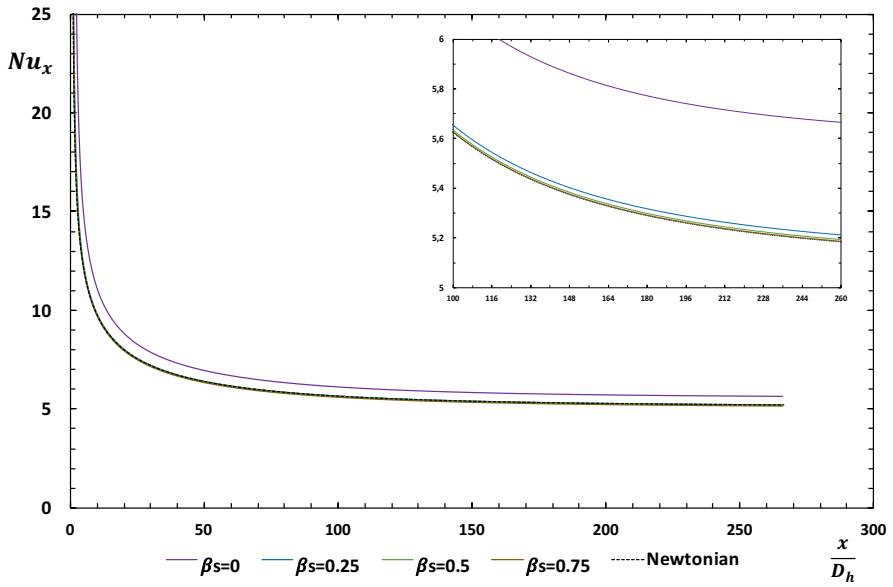

Figure 4.10: Contribution of the Newtonian solvent to PTT model. $De = 20$ and $\xi = 0$.

As reported in the previous testcase ($De = 10$), if the fluid has zero second stress coefficient, any quantity of Newtonian solvent added to the polymeric liquid completely ruins the effects of shear-thinning on the heat transfer. All the solutions tested for this value of *Deborah* tend to the Newtonian value for the *Nusselt* number. In resemblance to what was tested for $De = 10$, it was also carried out other simulations to test the influence of the ξ parameter of the PTT model for $De = 20$. The results for a range of ξ varying from 0 to 0.05 are presented in figures 4.11, 4.12 and 4.13, for β_s of 0.25, 0.5 and 0.75, respectively.

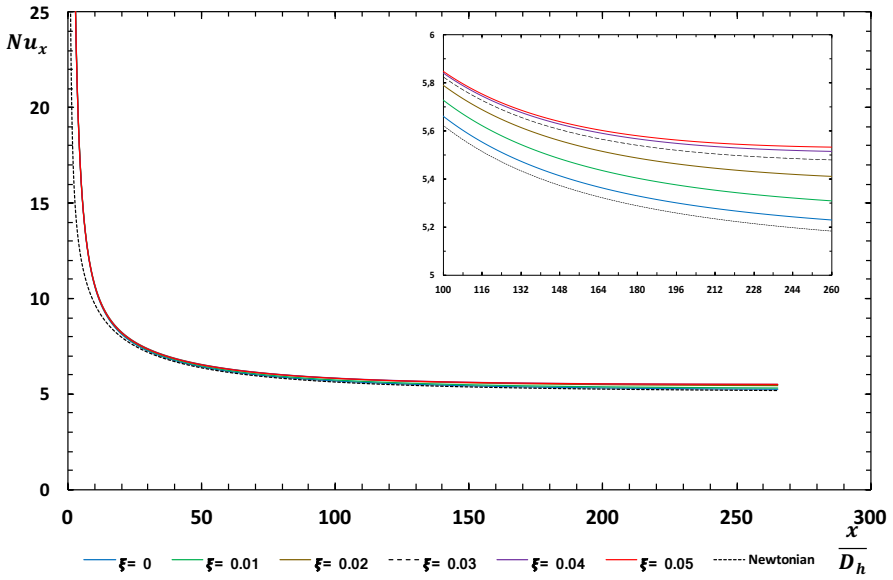

Figure 4.11: Effect of the ξ parameter on a PTT fluid, with a Newtonian solvent contribution. $De = 20$, $\varepsilon = 0.25$, $\beta_s = 0.25$.

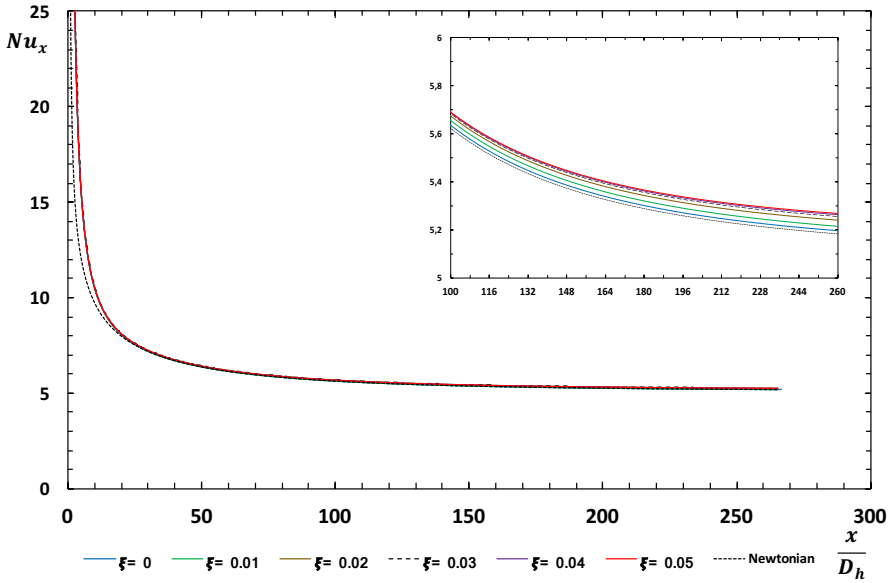

Figure 4.12: Effect of the ξ parameter on a PTT fluid, with a Newtonian solvent contribution.$De = 20$, $\varepsilon = 0.25$, $\beta_s = 0.5$.

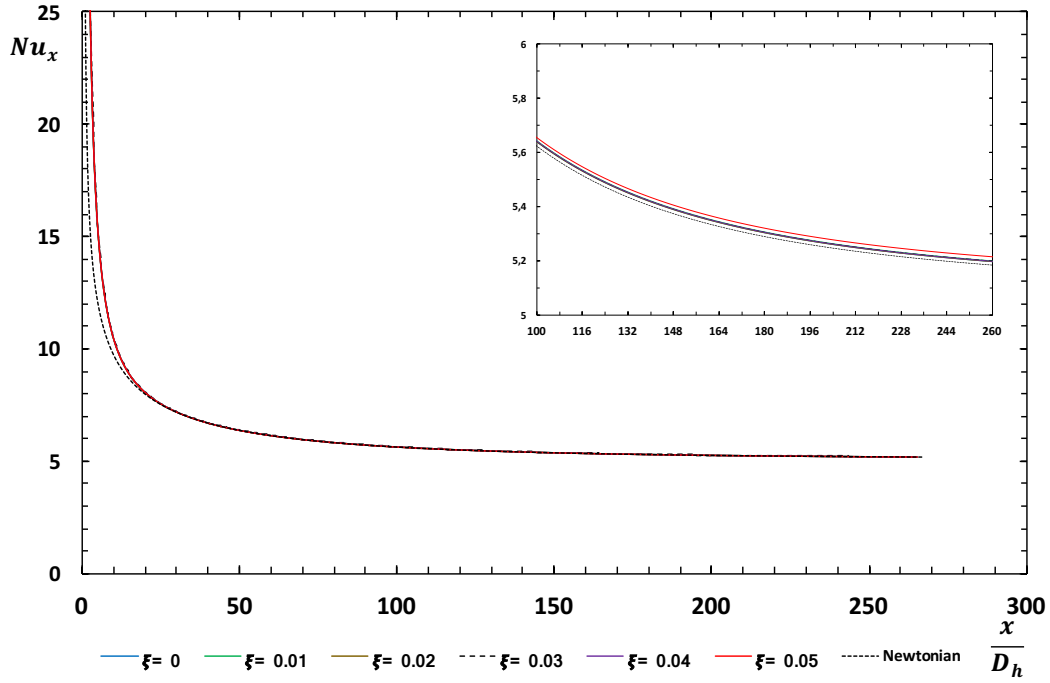

Figure 4.13: Effect of the ξ parameter on a PTT fluid, with a Newtonian solvent contribution. $De = 20$, $\varepsilon = 0.25$, $\beta_s = 0.75$.

Contrary to what was observed in the cases where $De = 10$, the asymptotic behavior of the axial *Nusselt* number does not appear to increase along the axial length of the duct. For $De = 20$, the slope of the curves where $\xi \neq 0$ are practically zero. This appears to imply that the increase in elasticity of the fluid has a stabilizing effect on the heat transfer coefficient of the models. In table 4.7, it is presented the percentage of increase in Nu compared to the Newtonian value.

Table 4.7: Percentage of increase in Nu, by comparison to a Newtonian fluid. $De = 20$,$\varepsilon = 0.25$

β_s	$\xi = 0.01$	$\xi = 0.02$	$\xi = 0.03$	$\xi = 0.04$	$\xi = 0.05$
0.25	2.37 %	4.25 %	5.51 %	6.16 %	6.49 %
0.5	0.58 %	1.05 %	1.34 %	1.5 %	1.58 %
0.75	0.28 %	0.57 %	0.74 %	0.78 %	0.82 %

Although the presence of strong amounts of Newtonian solvent ($\beta_s = 0.5$ and $\beta_s = 0.75$) had a ruining effect on the heat transfer behavior, for the case where the *Deborah* number was low ($De = 10$), in these cases, where *Deborah* was twice the value reported in section 4.2.2.1, the increase in the fully developed *Nusselt* number was even smaller compared to the values presented in table 4.6.

4.2.2.3 De=100 and De=200

To check if the Newtonian solvent added to the fluid, would have the same impact on heat transfer, simulations were carried out for cases where the relaxation time λ of the fluid was 10 times the values registered in sections 4.2.2.1 and 4.2.2.2. However, it was not possible to achieve convergence for these cases with the presence of secondary flow. The results for the simplified PTT model, are presented in figures 4.14 and 4.15, with $De = 100$ and $De = 200$.

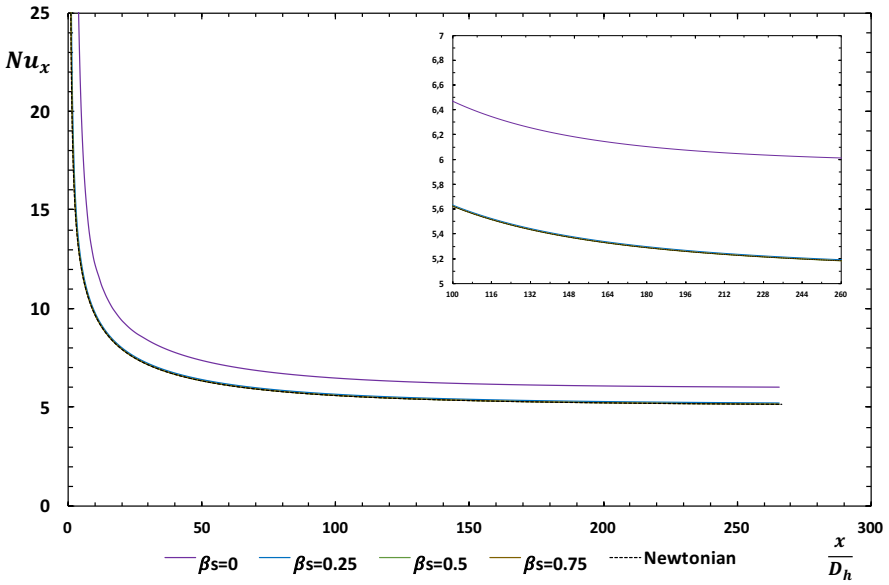

Figure 4.14: Contribution of the Newtonian solvent to PTT model. $De = 100$ and $\xi = 0$.

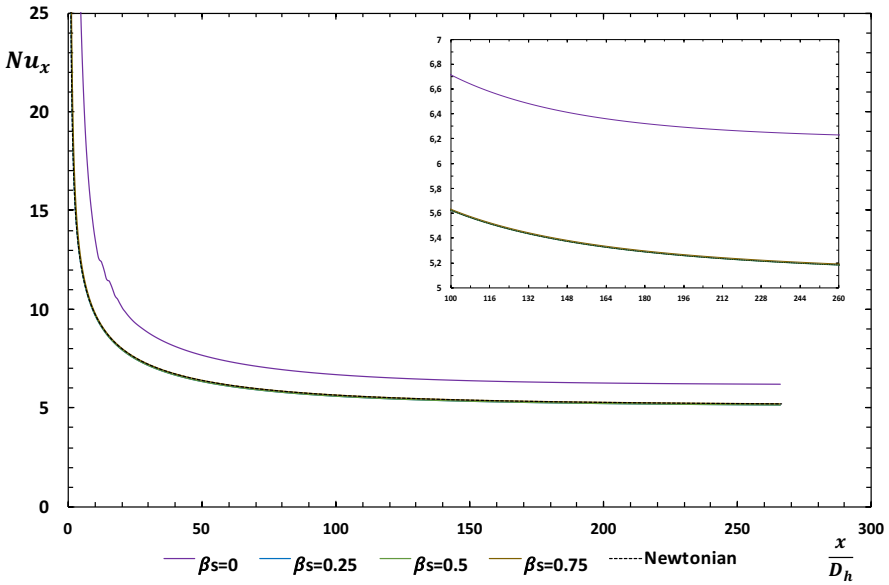

Figure 4.15: Contribution of the Newtonian solvent to PTT model. $De = 200$ and $\xi = 0$.

As it can be observed, the same effects were registered as in the cases reported in sections 4.2.2.1 and 4.2.2.2. In the absence of secondary flow motion, and independently of the elasticity of the fluid, it would appear that the heat transfer behavior always tends to the same behavior as a Newtonian fluid. There is nothing much that can be done for these cases, because the convergence time needed to test for secondary flow motion is not compatible with the time available to finish this dissertation.

Chapter 5

Conclusions and Future Work

This chapter is devoted to present the conclusions in this thesis. Given the reported values for the heat transfer behavior of the fluid, it would seem that the combined effects of viscous with non-linear and elastic behavior causes a definite increase in the heat transfer coefficient for viscoelastic fluids. The objective of this thesis was to do a parametric study of duct flow of a viscoelastic fluid governed by the PTT constitutive law to model the stresses. Due to the results obtained, the objective of this thesis was achieved.

5.1 Conclusions

The analysis of the heat transfer behavior of a viscoelastic liquid flowing in a duct was made by using the PTT constitutive model to predict the stress behavior of the fluid, when it is subjected to a fixed mass flux. The simulations were carried out in a duct with an aspect ratio AR of 2:1, considering both vertical side walls were adiabatic, and the top and bottom side walls were being heated.

The influence of heat transfer was evaluated for the influence of the elastic effects (by variation of De), by varying the non-linear behavior of the stresses (by varying both parameters ε and ξ of the PTT constitutive equation) and by adding the contribution of a Newtonian solvent to the model of the stresses (by variating β_s).

Two different axial lengths for the 2:1 duct were used. For the first, $L = 6.4$ m, a direct comparison with the numerical work of Peres et al. [4] was ascertained. In this duct, the contribution of a Newtonian solvent was low, $\beta_s \approx 0.04$, and the effects of both parameters ε and ξ were tested. It would appear that the given length of duct, for the *Reynolds* and *Prandtl* numbers reported in the paper, was not sufficient to obtain a stable value for the heat transfer coefficient of the fluid, if secondary motion exists. Not only the existence a second normal stress coefficient dramatically enhances the characteristic Nu of the fluid, it also generates a slope of growth in heat transfer, after asymptotically decreasing to a constant value. It was not possible to visualize fully developed thermal conditions in the fluid, except for the SPTT case, where the registeres increase in Nu, compared to the Newtonian solution, is of 39 %, for $De = 33.33$.

It would appear that varying the elongational parameter (ε) of the PTT model has no effect on the heat transfer behavior, except for the case where secondary motion was low. For zero secondary flow, the effect of ε is null. However, in the intermediate region between $\xi = 0$ and $\xi = 0.02$, the heat transfer coefficient varies with the elongationality of the fluid, and slightly decreases with increasing value of ε. It appear that, by increasing the magnitude of secondary flow ($\xi = 0.02$), varying the elongationality of the fluid appears to have almost no effect, once again. However, the same behavior for the cases where $\xi = 0.01$ are the same, *Nusselt* increases with increasing elongationality.

In the next set of simulations tested using the viscoelastic model, *Reynolds* and *Prandtl* were severely decreased, in order to try and guarantee fully developed dynamic and thermal conditions. The length of the duct was also diminished, $L = 3.2$ m, in order to provide more accurate results. The mesh used to generate the boundaries of the flow, mesh B, was tested for the same thermal boundary conditions as the ones tested in mesh A, achieving results of 0.4 % for the *Nusselt* number.

The influence of elastic effects was first tested for a SPTT fluid ($\xi = 0$) with $\varepsilon = 0.25$. The results show that, even the presence of small elasticity, $De = 10$, causes an increase of almost 9 % comparing with the corresponding Newtonian analytical value, reaching an enhancement of about 20 %, for large elastic effects ($De = 200$).

The influence of adding a Newtonian solvent to the solution shows that, if no secondary motion exists, the asymptotical *Nusselt* number is the same as for a Newtonian fluid. In fact, even for the lowest contribution of Newtonian solvent, $\beta_s = 0.25$, the heat transfer coefficient for the viscoelastic fluid is the same as for a fluid of Newtonian characteristics. This appears to be true, no matter the intensity of the elastic effects. As seen for $De = 100$ and $De = 200$, for any value of β_s, the solution always tends to the Newtonian case.

Combining the existence of secondary motion in the fluid, $\xi \neq 0$, with the different values of β_s for which the model was tested, it could be observed a slight increase in the heat transfer coefficient. The influence of ξ, with varying β_s, was tested for the two lowest *Deborah* numbers assumed in the trial runs, 10 and 20.

For $De = 10$, it would appear that moderate and high concentrations of Newtonian solvent, $\beta_s = 0.5$ and $\beta_s = 0.75$ eliminate the growth caused by increasing the ξ parameter of the PTT model. For moderate values of β_s, 0.5, even the strongest presence of secondary motion, $\xi = 0.05$, registers an increase of only about 3 % by comparison with the Newtonian value of 5.2. As for the more dilute solution, $\beta_s = 0.75$, the increase is less than 1 %. However, for the more concentrated solution of polymeric liquid, $\beta_s = 0.25$, a similar slope of growth was registered, as for the models tested with $\beta_s \approx 0.04$, and the highest increase in the heat transfer behavior registered for theses cases was of 13.4%, for $\xi = 0.05$.

In the case where $De = 20$, the effects of β_s apparently eliminate any slope of growth in Nu due to secondary motion of the fluid. In fact, for the highest contribution of polymer viscosity, $\beta_s = 0.25$, the elasticity of the fluid appeared to

have a soothing behavior to the thermal entrance length, thus allowing the fluid to achieve fully developed conditions, for any value of ξ. Contrary to what was actually expected, the heat transfer coefficient obtained in fully developed conditions was actually lower, comparing with the lowest value of De, independently of the intensity of the secondary flow arising in the fluid. In fact, for the highest values of β_s (0.5 and 0.75), the deviation from the analytical value for the Newtonian case is extremely small, almost identical.

Due to extended amount of time needed to achieve convergence for the numerical simulations with the largest values of elasticity, it cannot be concluded that the difference in effects verified between the two cases of $De = 10$ and $De = 20$ will remain the same independently of the *Deborah* number of the flow, or if this pattern will change.

It was not possible to simulate for higher values of ξ, since the computational times needed for the simulations to achieve convergence were extremely high. For the highest values of ξ parameter presented in this work, it could take about three to four weeks before convergence could be achieved.

5.2 Future Work

For future works, it is recommended to investigate the effects of a Newtonian solvent in smaller quantities, closer to zero, to better quantify the influence on the heat transfer behavior of the flow, and how much it differs from the results reported in this thesis. It is also suggested the limiting case where $\beta_s = 0$, but with a non-zero second stress coefficient, as a means of characterizing the heat transfer coefficient in polymer melts, and how secondary flow affects the heat transfer behavior.

The influence of buoyancy in viscoelastic fluids should be investigated, as the effects of natural convection in laminar flow in rectangular ducts need to be quantified, to better predict the heat transfer behavior of the flow.

Finally, investigation on different aspect ratios for rectangular ducts, and different configurations for wall heating should be studied. As the verification for the case where all walls are being heated was aldready made in this work, it is suggested that the case where all walls are being heated should be tested.

Bibliography

[1] F. T. Pinho. Cálculo de escoamentos de fluidos não Newtonianos em regime laminar: Desenvolvimentos e aplicações recentes da metodologia dos volumes finitos. FEUP, 2003.

[2] N. Phan-Thien and R. I. Tanner. A new constitutive equation derived from network theory. Journal of Non-Newtonian Fluid Mechanics, 2(4):353 – 365, 1977.

[3] N. Phan-Thien. A Nonlinear Network Viscoelastic Model. Journal of Rheology, 22(3):259–283, 1978.

[4] N. Peres, A. M. Afonso, M. A. Alves, and F. T. Pinho. Heat transfer enhancement in laminar flow of viscoelastic fluids through rectangular ducts. In CMNE, 2009.

[5] F. M. White. Fluid Mechanics. McGraw-Hill, 2011.

[6] F.M. White. Viscous Fluid Flow. McGraw-Hill, 2005.

[7] R. B. Bird, R. C. Armstrong, and O. Hassager. Dynamics of Polymeric Liquids, Vol.1: Fluid dynamics. John Wiley & Sons, Inc., 1987.

[8] T. L. Bergman, A. S. Lavine, F. P. Incropera, and D. P. Dewitt. Fundamentals of Heat and Mass Transfer. John Wiley & Sons, Inc., 7th edition, 2011.

[9] A. B. Metzner and J. C. Reed. Flow of Non-newtonian Fluids-Correlation of the Laminar, Transition and Turbulent-flow Regions. A.I.Ch.E Journal, 1(4):433–440, 1955.

[10] R. B. Bird and P. J. Carreau. A nonlinear viscoelastic model for polymer solutions and melts—i. Chemical Engineering Science, 23(5):427 – 434, 1968.

[11] K. Yasuda, R. C. Armstrong, and R. E. Cohen. Shear flow properties of concentrated solutions of linear and star branched polystyrenes. Rheologica Acta, 20(2):163–178, 1981.

[12] J. Meissner. Basic parameters, melt rheology, processing and end-use of three similar low density polyethylene samples. Pure and Applied Chemistry, 42(4), 1975.

[13] J. L. Ericksen. Overdetermination of the speed in rectilinear motion of non-newtonian fluids. Quarterly of Applied Mathematics, 14(3):318–321, 1956.

[14] A. E. Green and R. S. Rivlin. Steady flow of non-newtonian fluids through tubes. Transactions of the Society of Rheology, 14:299–308, 1956.

[15] R. S. Rivlin and J. L. Erickesn. Stress-deformation relations for isotropic materials. Journal of Rational Mechanics and Analysis, 4(2), March 1955.

[16] J. A. Wheeler and E. H. Wissler. The friction factor–reynolds number relation for the steady flow of pseudoplastic fluids through rectangular ducts. part i. theory. AIChE Journal, 11(2):207–212, 1965.

[17] J. A. Wheeler and E. H. Wissler. The friction factor–reynolds number relation for the steady flow of pseudoplastic fluids through rectangular ducts. part ii. experimental results. AIChE Journal, 11(2):212–216, 1965.

[18] J. A. Wheeler and E. H. Wissler. Steady flow of non-newtonian fluids in a square duct. Transactions of the Society of Rheology, 10(1):353–367, 1966.

[19] P. Townsend, K. Walters, and W. M. Waterhouse. Secondary flows in pipes of square cross-section and the measurement of the second normal stress difference. Journal of Non-Newtonian Fluid Mechanics, 1(2):107–123, 1976.

[20] B. Gervang and P. S. Larsen. Secondary flows in straight ducts of rectangular cross section. Journal of Non-Newtonian Fluid Mechanics, 39(3):217–237, 1991.

[21] S.X. Gao and J.P. Hartnett. Steady flow of non-newtonian fluids through rectangular ducts. International Communications in Heat and Mass Transfer, 20(2):197 – 210, 1993.

[22] S. C. Xue, N. Phan-Thien, and R.I. Tanner. Numerical study of secondary flows of viscoelastic fluid in straight pipes by an implicit finite volume method. Journal of Non-Newtonian Fluid Mechanics, 59(2):191 – 213, 1995.

[23] G. W. M. Peters and F. P. T. Braaijens. Modelling of non-isothermal viscoelastic flows. Journal of Non-Newtonian Fluid Mechanics, 68:205–224, 1997.

[24] P. Wapperom. Non-isothermal flows of viscoealastic fluids, Thermodynamics, analysis and numerical simulation. PhD thesis, Delft University of Technology, 1995.

[25] P. Wapperom and M. A. Hulsen. Thermodynamics of viscoelastic fluids : The temperature equation. Journal of Rheology, 42(5):999–1019, 1998.

[26] A.B. Metzner. Heat transfer in non-newtonian fluids. In James P. Hartnett and Thomas F. Irvine, editors, Advances in Heat Transfer, volume 2, pages 357 – 397. Elsevier, 1965.

[27] J. P. Hartnett and M. Kostic. Heat transfer to newtonian and non-newtonian fluids in rectangular ducts. In James P. Hartnett and Thomas F. Irvine, editors, Advances in Heat Transfer, volume 19, pages 247 – 356. Elsevier, 1989.

[28] J. P. Hartnett and M. Kostic. Heat transfer to a viscoelastic fluid in laminar flow through a rectangular channel. International Journal of Heat and Mass Transfer, 28(6):1147–1155, 1985.

[29] P. Wibulswas. Laminar Flow Heat Transfer in Non-circular Ducts. PhD thesis, University College London, 1966.

[30] B. K. Rao. Laminar mixed convection heat transfer to viscoelastic fluids in a 5:1 rectangular channel. International Journal of Heat and Fluid Flow, 10(4):334–338, 1989.

[31] S. X. Gao and J. P. Hartnett. Heat transfer behavior of reiner-rivlin fluids in rectangular ducts. International Journal of Heat and Mass Transfer, 39(6):1317 – 1324, 1996.

[32] P. Payvar. Heat transfer enhancement in laminar flow of viscoelastic fluids through rectangular ducts. International Journal of Heat and Mass Transfer, 40(3):745–756, 1997.

[33] M. Kostic. Heat transfer and hydrodynamics of water and viscoelastic fluid flow in a rectangular duct. PhD thesis, University of Illinois at Chicago, IL, 1984.

[34] F. T. Pinho and P. J. Oliveira. Analysis of forced convection in pipes and channels with the simplifed Phan-Thien and Tanner fluid. International Journal of Heat and Mass Transfer, 43:2273–2287, 2000.

[35] P. M. Coelho, F. T. Pinho, and P. J. Oliveira. Fully developed forced convection of the phan-thien–tanner fluid in ducts with a constant wall temperature. International journal of heat and mass transfer, 45(7):1413–1423, 2002.

[36] P. J. Oliveira, F. T. Pinho, and G. A. Pinto. Numerical simulation of non-linear elastic flows with a general collocated finite-volume method. Journal of Non-Newtonian Fluid Mechanics, 79(1):1–43, 1998.

[37] C. D. Eggleton, T. H. Pulliam, and J. H. Ferziger. Numerical simulation of viscoelastic flow using flux difference splitting at moderate reynolds numbers. Journal of Non-Newtonian Fluid Mechanics, 64(2–3):269 – 298, 1996.

[38] H. H. Hu and D. D. Joseph. Numerical simulation of viscoelastic flow past a cylinder. Journal of Non-Newtonian Fluid Mechanics, 37(2):347 – 377, 1990.

[39] P. Y. Huang and J. Feng. Wall effects on the flow of viscoelastic fluids around a circular cylinder. Journal of Non-Newtonian Fluid Mechanics, 60(2):179 – 198, 1995.

[40] V. Delvaux and M.J. Crochet. Numerical prediction of anomalous transport properties in viscoelastic flow. Journal of Non-Newtonian Fluid Mechanics, 37(2–3):297 – 315, 1990.

[41] J. M. Nóbrega, F. T. Pinho, P. J. Oliveira, and O. S. Carneiro. Accounting for temperature-dependent properties in viscoelastic duct flows. International Journal of Heat and Mass Transfer, 47(6-7):1141–1158, 2004.

[42] R.K. Shah and A. L. London. Laminar Flow Forced Convection In Ducts. In Advances In Heat Transfer, page 482. Academic Press Inc., 1978.

[43] P.M. Coelho, F. T. Pinho, and P.J. Oliveira. Thermal entry flow for a viscoelastic fluid: the graetz problem for the {PTT} model. International Journal of Heat and Mass Transfer, 46(20):3865 – 3880, 2003.

[44] A. M. S. Cavadas. Hidrodinâmica de jactos de impacto confinados escoamento de fluidos newtonianos e não newtonianos. PhD thesis, Universidade do Porto, 2008.

[45] C. M. Rhie and W. L. Chow. Numerical study of the turbulent flow past an airfoil with trailing edge separation. AIAA journal, 21(11):1525–1532, 1983.

[46] M. A. Alves, P. J. Oliveira, and F. T. Pinho. A convergent and universally bounded interpolation scheme for the treatment of advection. International Journal for Numerical Methods in Fluids, 41(1):47–75, 2003.

[47] P. J. Oliveira and F. T. Pinho. Analytical solution for fully developed channel and pipe flow of Phan-Thien–Tanner fluids. Journal of Fluid Mechanics, 387:271–280, 1999.

[48] M. A. Alves, F. T. Pinho, and P. J. Oliveira. Study of steady pipe and channel flows of a single-mode Phan-Thien-Tanner fluid. Journal of Non-Newtonian Fluid Mechanics, 101(1-3):55–76, 2001.

[49] M. Reiner. The deborah number. Physics today, 17(1):62, 1964.

Appendix A

Non-dimensional parameters

The flow of a fluid can be characterized by two different regimes, laminar and turbulent. The major parameter that quantifies which regime is occurring in fluid flow is the *Reynolds* number, equation (A.1). It is essentially a balance of the ratio between the pressure forces to the viscous forces acting in fluid flow, given by

$$Re = \frac{\rho \bar{u} L}{\eta}, \tag{A.1}$$

where ρ is the density, $\bar{u}$ is the average velocity of the fluid and η is the dynamic viscosity. L is the characteristic length of the geometry in which the fluid is flowing. For channel flow, the characteristic length is usually assumed as four times the half-width of the channel h ($L = 4h$), whereas for non-circular ducts, L corresponds to the hydraulic diameter D_h, defined as the ratio between the cross-sectional over the wetted perimeter ($D_H = \frac{A_C}{P_W}$).

Another parameter of importance is the friction factor *f*. It corresponds to the normalized wall shear stress occurring on the walls of the geometry in which the fluid is flowing. It can be defined in two ways, the fanning friction factor, equation (A.2), or the Darcy friction factor, equation (A.3),

$$f_f = \frac{2\tau_w}{\rho \bar{u}^2} \tag{A.2}$$

$$f_D = \frac{8\tau_w}{\rho \bar{u}^2} \tag{A.3}$$

where is τ_w is the average shear stress on the wall.

As it was referenced before, each viscoelastic fluid possesses a relaxation time λ associated to it. In non-Newtonian liquids, this parameter is often presented in normalized form, the *Deborah* number, equation (A.4).

$$De = \frac{\lambda}{t_{flow}} \tag{A.4}$$

where t_{flow} is taken to be a characteristic time of the flow. This is often defined as the ratio of the average velocity $\bar{u}$ of the fluid with the characteristic length L ($t_{flow} = \bar{u}/L$), thus defining De as follows in equation (A.5).

$$De = \frac{\lambda \bar{u}}{L} \tag{A.5}$$

The *Deborah* number can be interpreted as the ratio of the magnitude of the elastic forces to that of viscous forces [7]. This interpretation immediately implies that the main difference between solid and liquid material comes from the magnitude of *De*. If *De* is very large, the material, for all pratical purposes, behaves as a solid ($\lambda \to \infty$). If the opposite case is observed, then the material behaves as a liquid ($\lambda \to 0$) [49].

The PTT model describes the polymer contribution to the stress tensor, and it also may be considered an extra stress term from a Newtonian solvent contribution. The total stress tensor in the fluid may then exhibit two different viscosity

contributions, the one from the stress terms of the polymer, η_p, and the one from the solvent, η_s. It is common to define β_s, as the ratio of the Newtonian solvent to the total viscosity of the model, equation (A.6),

$$\beta_s = \frac{\eta_s}{\eta_0} \tag{A.6}$$

where $\eta_0 = \eta_s + \eta_p$ is the sum of the viscosity of the polymeric liquid with the viscosity for the Newtonian solvent.

For any fluid, the rate of heat transfer through convection in fluid flow is characterized by an important dimensional parameter: The *Nusselt* number, defined as the ratio of the convective conduction h_c to the molecular conduction k/L [42], equation (A.7),

$$Nu = \frac{h_c L}{k} \tag{A.7}$$

where L is the characteristic length. As it can be easily seen, the *Nusselt* number corresponds to the normalized form of the heat transfer coefficient of a fluid.

At this point, it is important to introduce a second non-dimensional parameter. The *Prandtl* number, defined as the ratio of the momentum diffusivity to the thermal diffusivity, equation (A.8),

$$Pr = \frac{\nu}{\alpha} = \frac{\eta C}{k} \tag{A.8}$$

where ν is the kinematic viscosity($\nu = \eta/\rho$) and α is the thermal diffusivity ($\alpha = \rho C/k$). The importance of this non-dimensional number relies in the fact that it measures the relative growth of the velocity and thermal boundary layers. So, if $Pr < 1$ means that the energy diffusion rate is larger than the momentum difusion rate, i.e, the fluid becomes thermally developed before its dynamics reach fully developed condition. The opposite can be observed for $Pr > 1$, and for $Pr = 1$ both boundary layers develop simultaneously.